2014-01-01

Characterization Of The Disulfide In The Ectodomain Of Anthrax Toxin Receptor 2

Pedro Raymundo Jacquez
University of Texas at El Paso, prjacquez@miners.utep.edu

CHARACTERIZATION OF THE DISULFIDE BONDS IN THE ECTODOMAIN OF ANTHRAX TOXIN RECEPTOR 2

PEDRO RAYMUNDO JACQUEZ

Department of Biological Sciences

APPROVED:

Jianjun Sun, Ph.D., Chair

Marc B. Cox, PhD., Advocate

Siddhartha Das, Ph.D.

Jianying Zhang, Ph.D.

Chuan Xiao, PhD.

Charles Ambler, Ph.D.
Dean of the Graduate School

Dedication

I would like to dedicate this accomplishment to my family especially my mother, Maria Reyes Valenzuela de Jacquez, and most importantly, my beautiful and amazing daughter, Romina Jacquez.

CHARACTERIZATION OF THE DISULFIDE BONDS IN THE ECTODOMAIN OF ANTHRAX TOXIN RECEPTOR 2

by

Pedro Raymundo Jacquez, B.S.M.

DISSERTATION

Presented to the Faculty of the Graduate School of

The University of Texas at El Paso

in Partial Fulfillment

of the Requirements

for the Degree of

Doctor of Philosophy

Department of Biological Sciences

THE UNIVERSITY OF TEXAS AT EL PASO

December 2014

Acknowledgements

First I would like to thank each member of my dissertation committee. I would like to thank Dr. Renato Aguilera for giving me the opportunity to be part of the University of Texas at El Paso Biological Sciences Department research family in the doctoral degree program, I am very much grateful to him. I would also like to thank, Drs. Jianying Zhang and Dr. Chuan Xiao for their support and guidance throughout my dissertation project. Furthermore, I am very grateful to have met my undergraduate advisor, Dr. Siddhartha Das, since he is responsible of helping and motivating me to pursue such honorary degree. He has been a great mentor and friend for many years, and I have grown to care for him very much. Next, I would like to thank my advocate and great friend Dr. Marc B. Cox. Dr. Cox has been really helpful in respect to all of my graduate career and personal life. He has also expressed his confidence in me in becoming a great scientist. I have really enjoyed being close to him as his student but also as a friend. Lastly, I would like to thank my dissertation mentor, Dr. Jianjun Sun. I have no way on repaying Dr. Sun for everything he has done for me. He has given me the best support any student can ask for, and has trained me to become a competent Ph.D. student. I believe Dr. Sun has become more than a mentor to me, more like a scientific brother. I will forever be grateful to Dr. Sun.

I would also like to thank the entire graduate, undergraduate and staff that have been part of Dr. Sun's laboratory over the past five years. I am thankful for their support, help and care they have shared with me during this time. I would also like to thank the Biological Sciences Department faculty, staff, especially Ms. Annette Vazquez, and students, for all of their help and support during my graduate career.

Lastly, I would like to thank my friends and family that have supported me since I started my studies. I would like to thank my sisters, Irma, Laura, Teresa and Lorena Jacquez, brothers in law, nieces and nephews, for their unconditional support, love and care during my science career. In addition, I cannot express enough the gratitude towards my parents, Pedro Raymundo Jacquez Villalobos and Maria Reyes Valenzuela de Jacquez, for their commitment to support, love and provide for me during my life. I could not have accomplished anything with the love, care and support coming from my parents. Finally, all of my accomplishments are entirely dedicated to the love of my life, my daughter Romina Jacquez. I am grateful in having such a beautiful and intelligent daughter that has motivated me to succeed in life and be an exemplary father to her.

Abstract

Anthrax toxin receptors act as molecular clamps or switches that control anthrax toxin entry, pH-dependent pore formation, and translocation of enzymatic moieties across the endosomal membranes. The ectodomain of anthrax toxin receptor 2 (ANTXR2) is composed of a von Willebrand factor A (VWA) domain that binds to anthrax toxin protective antigen (PA) and a newly defined immunoglobulin-like (Ig) domain, in which the disulfide bonds are required for PA pore formation and for the folding of ANTXR2. While the VWA domain has been well characterized, the structure and function of the whole ectodomain (VWA-Ig) are poorly defined, this is mainly due to the limited production of the soluble recombinant protein of the ectodomain. In order to overcome this, the ANTXR2 ectodomain was fused to the C-terminus of bacterial Trigger Factor (TF), a chaperone that mediates the ribosome-associated, co-translational folding of newly synthesized polypeptides in E. coli. Under the control of a cold shock promoter, the fusion protein was overly expressed as a dominant soluble protein at a low temperature in the oxidative cytoplasm of Origami B cells, where formation of the disulfide bonds is favored. Through a series of chromatography, the ANTXR2 ectodomain was purified into homogeneity. The purified ectodomain is functional in binding to PA and mediating PA pore formation on the liposomal membranes, and the yield is applicable for future biochemical and structural characterization. We have also previously reported that reduction of the disulfide bonds in the immunoglobulin-like (Ig) domain of the anthrax toxin receptor 2 (ANTXR2) inhibited function of the protective antigen (PA) pore, as measured by release of K^+ ions from liposomes and from Chinese hamster ovary (CHO) cells, or by the pore-mediated translocation of a model substrate

across the plasma membranes. Therefore, the disulfide linkage in the Ig domain was identified as Cys255-Cys279 and Cys230-Cys315. Deletion of C255-C279, but not C230-C315, inhibited the PA pore-induced release of the fluorescence dyes from the liposomes, suggesting that C255-C279 is essential for PA pore function. Further, we found that deletion of C255-C279 did not affect PA prepore-to-pore conversion, but inhibited PA pore membrane insertion by trapping the PA membrane-inserting loops in proteinaceous hydrophobic pockets. Fluorescence spectra of Try59, a residue adjacent to the PA-binding motif in von Willebrand factor A (VWA) domain of ANTXR2 showed that deletion of C255-C279 resulted in a significant conformational change on the receptor ectodomain. The disulfide deletion-induced conformational change on the VWA domain was further confirmed by single-particle 3D reconstruction of the negatively stained PA-receptor heptameric complexes. This study elucidates a novel mechanism for anthrax inhibition through modulating receptor disulfide bonds.

Table of Contents

List of Tables

List of Figures

List of Illustrations

Chapter 1: Introduction

1.1 *Bacillus anthracis*

Anthrax, a lethal disease of humans and animals, is caused by the gram-positive spore-forming eubacterium, *Bacillus anthracis* (1). It is the only obligate pathogen from the genus *Bacillus* that can grow in both aerobic and anaerobic conditions. The bacterial cell morphology includes a poly-D-gamma-glutamic acid protein capsule, which is unique in only a few bacterial species that has a width of 1–1.2 μm and a length of 3–5 μm (2, 3). *B. anthracis* forms endospores that begin to develop and mature inside the rod shape form and are known to be highly resilient, able to survive at extreme temperatures, low-nutrient environments, and harsh chemical treatment over decades or centuries. In addition, endospores are able to resist heat, drying, and many disinfectants, such as ethanol. Anthrax is a biological threat since it has been used as a biological weapon in both powdered and aerosol forms (4, 5).

Cellular division or endospore formation begins when either environmental conditions are favorable or the bacteria are exposed to radicals in the environment including oxygen. Once this occurs the bacteria will come out of a dormant state and begin to germinate. At this point the cells grow and divide, and produce anthrax protein toxins, which will be later discussed in details.

There are three types of anthrax infection, which are cutaneous, pulmonary, and gastrointestinal (6). The first is the most common form of the disease and is represented by localized, inflammatory, black, necrotic lesion. Pulmonary is the most severe form and can be described as sudden, massive chest edema followed by

cardiovascular shock (7). Finally, gastrointestinal anthrax, which is very rare in humans but very common in livestock, is still fatal when spores are ingested. The infection process begins when spores go through phagocytosis by macrophages where they germinate. Then bacteria escape from macrophages and multiply in tissues. Treatment at this point can be done with antibiotics, such as penicillin or others effective against Gram-positive bacteria (8). If infection is not treated, both bacteremia and toxin accumulation cause death approximately one week after infection. Currently, an effective anti-toxin is yet to be developed.

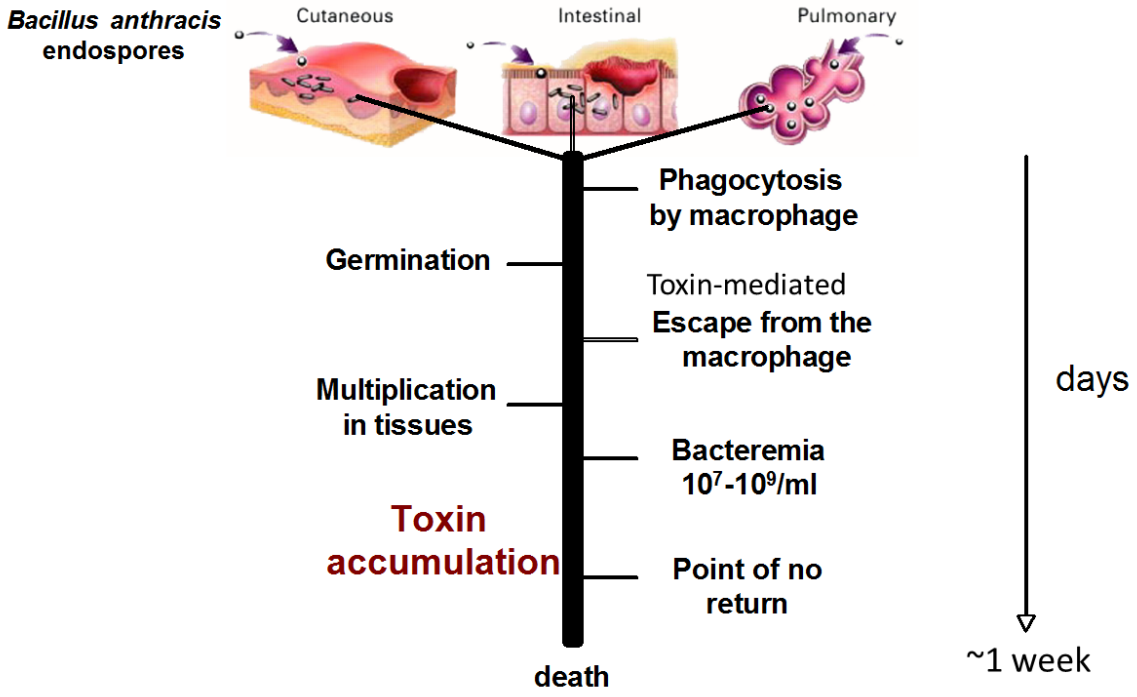

Illustration 1. Forms of anthrax disease and progression. As stated above there are three ways in which anthrax can cause disease, cutaneous, gastrointestinal and pulmonary. The diagram shows each important step in the course of the disease all the way to the "point of no return" and death.

1.2 Anthrax Toxin

B. anthracis genome consists of a single circular chromosome and two large plasmids, pXO1 and pXO2, which are required for full virulence (9, 10, 11). Both are part of two distinct plasmid families, in which pXO1 contains the genes coding for the anthrax toxin components, *pag (*protective antigen, PA), *lef* (lethal factor, LF), and *cya* (edema factor, EF), located within a pathogenicity island (PAI) (12). In addition, the PAI also encodes for both a transcriptional activator AtxA and a repressor PagR, which regulate the expression of the toxin (13, 14, 15, 16, and 17). On the other hand, pXO2 contains a five-gene operon (capBCADE) for the biosynthesis of the poly-γ-d-glutamic acid (polyglutamate) capsule as previously mentioned (18). This structure is very important since it aids the ability to evade the host immune system and also protects the vegetative cells from phagocytic killing by macrophages (19). pXO2 also has a PAI, in which the capsule operon and the transcriptional regulators AcpA and AcpB reside for the capsule expression, and the last two are also activated by the previously mentioned AtxA in pXO1 (14, 20, 21, 22).

Anthrax toxin is a tripartite A-B toxin, composed of two catalytic moieties, edema factor (EF) and lethal factor (LF), and a receptor binding/pore-forming moiety, protective antigen (PA) (23). LF is a zinc-dependent metalloprotease that cleaves members of the mitogen-activated protein kinase kinase family (all MKKs except MEK5) which inhibits the activation of this cellular pathway as well as other cellular metabolic processes. Once this occurs, LF is responsible of causing necrosis to the cell and therefore causing cell death. On the other hand, EF is a calmodulin and calcium–dependent adenylate cyclase that raises cyclic adenosine monophosphate levels within

the cell and causing loss of extracellular communication. Subsequently, the cell retains water which causes swelling and edema (25, 26).

1.3 Anthrax Toxicity

The first step of intoxication involves binding of the 83-kD PA (PA_{83}) to a cell-surface receptor, where it subsequently undergoes cleavage by furin or a furin-like protease to generate a 63-kD PA subunit (PA_{63}) that spontaneously assembles into a ring-like heptameric or octomeric structure, termed $PA(_{63})_7$ prepore (26). Then, both LF and EF bind to the PA heptamer. The entire toxin-receptor complex is internalized by receptor-mediated endocytosis (27, 28). The toxin complex is trafficked to the acidic endosomal compartment where low pH induces a conformational change in the $PA(_{63})_7$ prepore. This leads to the insertion of a 14 strand beta-barrel pore into the endosomal membrane that resembles a mushroom-shape form. Finally, both EF and LF are translocated into the cytoplasm where their catalytic activity takes place (29–31).

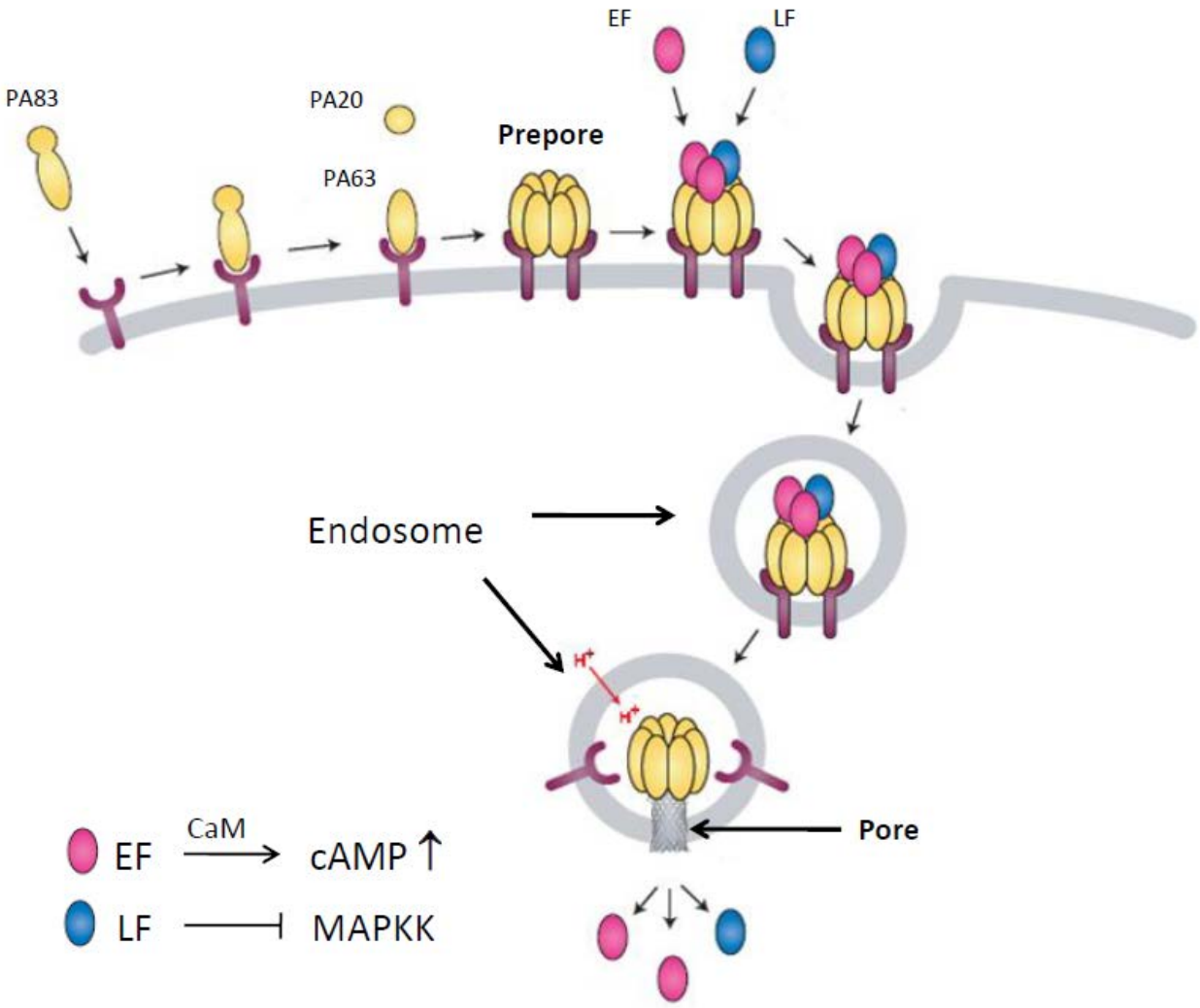

Leppla, 2000

Illustration 2. Anthrax toxin action once bound to a cell surface receptor.

1.4 Significance and Anthrax Vaccine

According to the Centers for Disease Control and Prevention (CDC), *B. anthracis* is classified as one of seven category A agents that are considered major threats as bioweapons (32). In 2001, the organism was used as a biological weapon targeting the Postal Service System in the United States of America, with 22 reported cases including the death of five people. Therefore, it is necessary to understand this bacterial agent and its pathogenic pathways in order to discover a readily available

therapeutic agent in case of a massive attack. So far, the U.S. Food and Drug Administration licensed an anthrax vaccine. This anthrax vaccine adsorbed (AVA; BioThrax) is composed of filtrate culture supernatant from *B. anthracis* and mostly contains PA as well as EF and LF, but in small detectable amounts (33, 34). The AVA vaccine is extremely reactogenic, and adverse reactions to the anthrax vaccine have been reported in both male and female receivers over long periods of time (35, 36, 37, 38, 39, 40, and 41). With this in mind, it is well understood that AVA is not an efficient preventive vaccine to the disease. In addition, other groups have reported library screening compounds, which inhibit anthrax toxin action, but not in a significant way (42, 43).

1.5 Anthrax Toxin Receptors

Anthrax toxicity and disease progression is highly mediated by two cellular receptors for PA interaction that have been identified: anthrax toxin receptor 1 (ANTXR1) and anthrax toxin receptor 2 (ANTXR2) (44, 45). ANTXR1 is also termed tumor endothelial marker 8 gene (TEM8), and ANTXR2 is termed as capillary morphogenesis protein two (CMG2). The two human receptors are 40% identical overall, but share 60% identity in the von Willebrand factor A (VWA)-like region where PA binding occurs (44, 45). Both ANTXR1 and ANTXR2 contain a domain that is homologous to the I domain of integrin receptors, which comprises a Rossmann-like α/β-fold with a metal-ion-dependent adhesion site (MIDAS) motif on the upper surface (46). Both receptors are type-I transmembrane proteins, comprising an extracellular domain (ectodomain), a single-pass transmembrane domain, and a cytoplasmic domain (23). Most human cells appear to express ANTXR2 (45) and ANTXR1 has been

reported to be expressed in human epithelial cells of the lungs, skin, intestines (47) and in endothelial cells (48).

In spite of the overall identity, ANTXR2 has a much higher affinity for PA (*Kd* = 0.170 nM compared to *Kd* = 130 nM for ANTXR1) (49). Crystal structures of the VWA domain of ANTXR2, and the PA-VWA complex have been determined (50, 51). Recently, it has been shown that the lethality of anthrax toxin for mice is primarily mediated by ANTXR2 and that ANTXR1 plays only a minor role (52).

1.6 Hypothesis

The goal of the project is to characterize the disulfide bonds within the ectodomain (extracellular domain) of ANTXR2. The ANTXR2 ectodomain is composed of two domains, an N-terminal VWA domain (termed R218 from now on) and an immunoglobulin-like factor domain (Ig). There are total seven cysteine residues in the ectodomain (termed R318 from now on), with three in the VWA domain and four in the Ig domain.

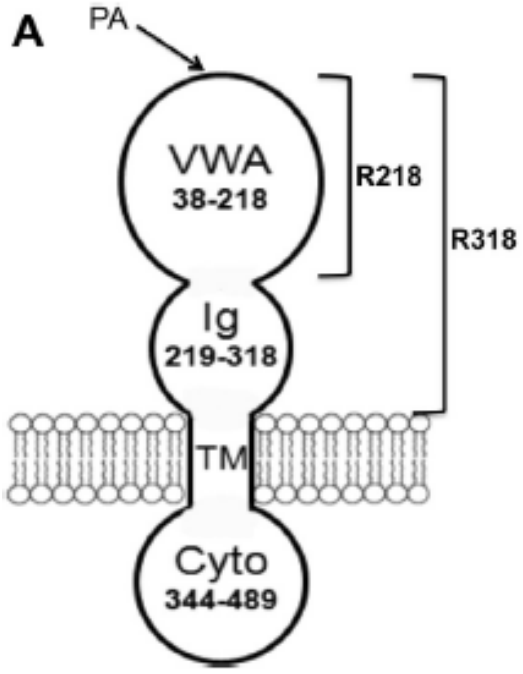

B

```
 38 SCRRAFDLYF VLDKSGSVAN NWIEIYNFVQ
 68 QLAERFVSPE MRLSFIVFSS QATIILPLTG
 98 DRGKISKGLE DLKRVSPVGE TYIHEGLKLA
128 NEQIQKAGGL KTSSIIIALT DGKLDGLVPS
158 YAEKEAKISR SLGASVYCVG VLDFEQAQLE
188 RIADSKEQVF PVKGGFQALK GIINSILAQS
218 CTEILELQPS SVCVGEEFQI VLSGRGFMLG
248 SRNGSVLCTY TVNETYTTSV KPVSVQLNSM
278 LCPAPILNKA GETLDVSVSF NGGKSVISGS
308 LIVTATECSN G
```

Illustration 3. Schematic of anthrax toxin receptor 2 (ANTXR2). A. ANTXR2 is composed of a PA-binding VWA domain (residues 38-218), an Ig domain (residues 219-318), a single-pass transmembrane domain (TM, 319-343) and a cytoplasmic domain (Cyto, 344-489). For simplicity, here VWA domain is termed as R218, and the whole ectodomain, VWA-Ig, is termed as R318. **B.** The amino acid sequence of ANTXR2 ectodomain, R318. The residues in the Ig domain are bolded and the Cys residues are highlighted.

Previous work has identified that there is a disulfide bond in the VWA domain, however, very little is known about the formation of disulfide bond(s) in the Ig domain (23). Furthermore, there has not been any type of structural characterization for R318. It is also not clear which disulfide bond(s) in R318 is required for toxin pathogenesis. Current work from Sun *et. al* (23) has suggested that the disulfide bonds in the ectodomain of R318 are required for the anthrax toxin action. **Therefore, the objective of this study is to determine the linkage pattern of the disulfide bonds, and identify the disulfide bond(s) that is/are required for anthrax toxin action.** These findings can give us insights into understanding the overall structure of R318 and the role of disulfide bonds in toxin action.

1.7 Specific Aims

-Specific Aim 1: Express and purify R318

-Specific Aim 2: Characterize and map the disulfide bonds of R318

-Specific aim 3: Investigate the role of the disulfide bonds of R318 in anthrax toxin action.

Chapter 2: Cloning, Expression and Purification of R318

2.1 Challenges of R318 expression and purification

Previous study has shown that although the VWA domain is highly soluble, R318 is expressed in *Escherichia coli* as an insoluble protein with only a minimal amount of soluble product. We believe this is due to mis-folding of the protein, probably caused by incorrect disulfide bond formation. Sun et. al., have previously expressed and purified the wild type (WT) soluble R318 protein using a maltose binding protein (MBP) as a fusion tag, but the yield is low (23).

Both immobilized metal affinity chromatography and size exclusion chromatography have been used in purifying R318, but the purification protocol has not yet been optimized. It is of great interest to produce a properly folded protein, which will be used in studies of the roles of the receptor disulfide bonds in anthrax toxin action.

2.2 Materials and Methods

2.2.1 R318 Cloning

R318 cDNA encoding residues 38-318 was amplified by PCR and inserted into a pMALc2x vector (NEB), at EcoRI and Hind III restriction sites **(Illustration 4)**. What is special about this vector is that R318 was expressed as a fusion with a N-terminal MBP (42kD) and a C-terminal 6 Histidine-tag. Therefore, the construct is termed, MBP-R318-His6 (~72kD). This construct is expressed in the cytoplasm of *E. coli* strain.

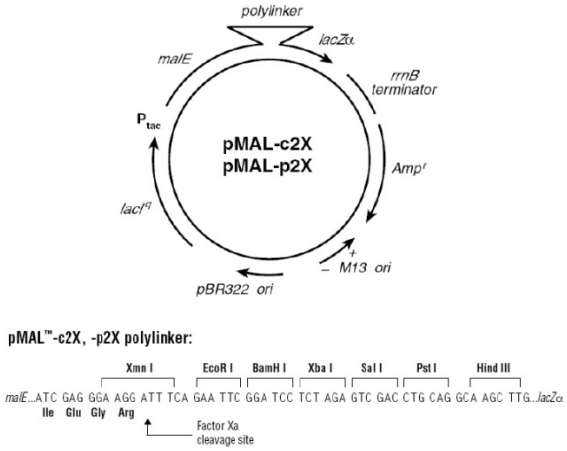

Illustration 4. pMALc2x expression vector. R318 was cloned into EcoRI and Hind III restriction sites. The vector expresses an MBP-fusion protein along with a strong "tac" promoter and the *malE* translation initiation signals, to give high levels of soluble proteins.

In addition, we have acquired *E. coli* Origami B (DE3) cells (Novagen) that are a specific strain carrying mutations in the genes of thioredoxin reductase (trxB) and glutathione reductase (gor), giving the cytoplasm an oxidized environment therefore favoring disulfide bond formation.

Alternatively, R318 was cloned into pCOLD-TF vector **(Illustration 5)** (Takara), using NdeI and XhoI restriction enzymes. This specific vector expresses Trigger Factor, which is a 48kD prokaryotic ribosome-associated chaperone protein, as a soluble fusion tag, and facilitates co-translational folding of newly expressed polypeptides. In addition, the vector has a cspA (cold shock protein A) promoter, which allows for up-regulation of target proteins at low temperatures. In addition, Trigger Factor carries a N-terminal 6-histidine tag for affinity purification. There are three protease cleavage sites (Factor Xα, Thrombin and **HRV** 3C) between Trigger Factor and the multiple cloning sites, so Trigger Factor can be cleaved off the target protein after purification.

Based on the characteristics of this vector we expressed the TF-R318 fusion protein at a low temperature (16˚C).

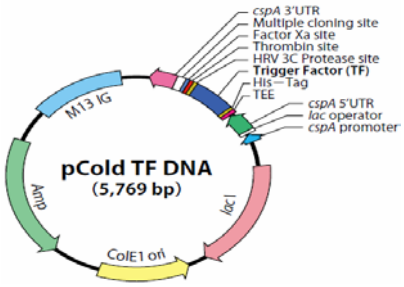

Illustration 5. pCOLD TF expression vector. R318 was cloned into NdeI and XhoI restriction sites. pCOLD expresses the chaperone Trigger Factor as a fusion tag and has a cspA (cold shock protein A) promoter which allows for up-regulation of target proteins at low temperatures.

Aside from these two R318 constructs, we also generated a number of different constructs to express R318 in Origami B (DE3) **(Table 1)**.

Table 1. List of the primers used to clone R318 into its respective expression vectors with given sequences and restriction enzymes.

Table 1
Primers used in this study.

Primers	Sequence (5′–3′)		Restriction sites
pET22b-R318-His_6	F	GGTGGTCATATGTCCTGCAGACGAGCCTTTG	Nde I/Xho I
	R	GGTGGTCTCGAGCCCGTTAGAACATTCTGTGGC	
pMal-c2x-R318-His_6	F	AGATCTGAATTCTCCTGCAGACGAGCCTTTG	EcoR I/Hind III
	R	ATGCAAGCTTGTGTCAATGGTGATGGTGATGATGCCCGTTAGAACA TTCTGTGGC	
pMal-c2x-R318	F	AGATCTGAATTCTCCTGCAGACGAGCCTTTG	EcoR I/Hind III
	R	ATGCAAGCTTGTGTCACCCGTTAGAACATTCTGTGGC	
pGEX4T-R318	F	AGATCTGAATTCTCCTGCAGACGAGCCTTTG	EcoR I/Xho I
	R	GGTGGTCTCGAGTCACCCGTTAGAACATTCTGTGGC	
pCOLD-TF-R318-His_6	F	GGTGGTCATATGTCCTGCAGACGAGCCTTTG	Nde I/Xho I
	R	GGTGGTCTCGAGTCAATGGTGATGGTGATGATGCCCGTTAGAACATTCTGTGGC	
pCOLD-TF-R318	F	GGTGGTCATATGTCCTGCAGACGAGCCTTTG	Nde I/Xho I
	R	GGTGGTCTCGAGTCACCCGTTAGAACATTCTGTGGC	

2.2.2 R318 cell transformation

Next we performed a transformation of all of the R318 plasmid constructs in Origami B (DE3) by placing 2 µL of DNA into 30 µL of cells into a 1.5 mL microcentrifuge tube and incubated on ice for 20 min. Then we heat shocked the sample at 42°C in an analog heatblock (VWR) for 45 seconds and then incubated on ice

for an additional 5 minutes. Then we added 970 µL of Luria-Bertani (LB) media and incubated at 37°C at 220 rpm for one hour in a 1585 Shaker Incubator (VWR). After one hour, we centrifuged the tube at 14,800rpm in Microfuge 16 centrifuge (Belkman Coultier) for 2 minutes and removed the media. Then we resuspended the cell pellet with 50 µL of ddH_2O and plated the cells in a LB agar plate with 100 µg/ml carbenicillin (Goldbio). The agar plate will be incubated overnight (<16 hours) at 37°C in a general purpose incubator (VWR).

2.2.3 R318 small- and large-scale cell growth, and induction

The following day we selected a colony and inoculated 10 mL of LB media with 100 µg/mL of carbenicillin and incubated at 37°C at 220 rpm overnight (<16hours). We did a small scale expression of the protein in 50mL of LB media in order to check for expression. On the following day we inoculated 49 mL of LB media with 1 mL of the overnight bacterial culture (1/50) and added 100 µg/mL of carbenicillin into a glass flask. Then, we placed the flask culture into a shaker incubator at its respective temperature at 220 rpm until the OD_{600} reaches 0.6-0.8. We then induced protein expression by adding Isopropyl β-D-1-thiogalactopyranoside (IPTG) at various concentrations and continue shaking for various length of time at indicated temperatures.

We first did titrations on induction temperature, IPTG concentrations, and time. Our temperature titrations included 37, 30, 25, 20, and 16°C. Our IPTG titrations included 1mM, 0.1mM, and 0.01mM. Finally, our time titrations ranged from 3, 6 hours, and overnight (<18hours) depending on the induction temperature. The titrated parameters for R318 expression were listed in Table 2:

Table 2. R318 different expression variables. First row represents temperature, first columns represent IPTG final concentrations and columns subsequent columns represent induction time course. o/n= overnight

R318	37°C	30°C	25°C	20°C	16°C
0.01mM IPTG	3 hours	6hours	o/n	o/n	o/n
0.1mM IPTG	3hours	6hours	o/n	o/n	o/n
1mM IPTG	3hours	6hours	o/n	o/n	o/n

For pCOLD TF-R318, we followed the same transformation, starter culture and small scale procedures as previously stated, but induced at 15°C for 18 hours with 1mM IPTG.

Large scale expression for purification purposes was done with 4-liters of LB media, and the cultures were induced at 15°C for 18 hours with 1mM IPTG once the OD_{600} reached 0.8. Cells were harvested and stored at -80°C.

2.2.4 R318 purification

For the purification process we resuspended the cell pellet in 3-5mL/g of cell pellet in Buffer A (20mM Tris HCl pH 7.3, 300mM NaCl, 10mM Imidazole) (Sigma Aldrich), 1mg/mL of lysozyme (Sigma Aldrich) and a pinch of phenylmethanesulfonylfluoride (Sigma Aldrich), and sonicated with a Vibracell VCX 750 sonicator (Sonics) using a 1/4inch sonicator tip at 40% amplitude for 30 minutes. Then we separated the total cell lysis into soluble and insoluble fractionations by centrifuging the cell extract in a Sorvall RC 6+ (Thermo Scientific) centrifuge in a SS34 rotor at 19,000rpms for one hour at 4°C. We collected the supernatant and discarded the insoluble pellet. We then prepared a General Electric 16XK (GE Healthcare) 75mL IMAC sepharose (GE Healthcare) 250mM Nickel Sulfate (Sigma Aldrich) charged column and equilibrated with 5 column volumes of Buffer A using a minipulse 3 peristaltic pump (Gilson) at 5ml/min. Once completed, we loaded our soluble fraction

into the column. In addition, the flow through fraction was also collected to test if our protein was being bound to the column. Once the entire soluble fraction sample was loaded into the column, we used a General Electric AKTA Fast Polypeptide Liquid Chromatography (GE Healthcare) to continue with the purification process.

The FPLC machine will be set to function at 5mL/min with a pressure no more than 0.3mPa. First the column was washed with 5 column volumes (375mL) of Buffer A, and then we set an elution gradient of 10% to 60% Buffer B (20mM Tris HCl pH 7.3, 300mM NaCl, 500mM Imidazole) (Sigma Aldrich) to elute our protein of interest. The AKTA FPLC device aliquots the elutions automatically and we checked for purification of our protein of interest on 12% SDS-PAGE gels.

In order to further purify our protein of interest, we continued with Size Exclusion Chromatography by using a General Electric XK 26/60 column (GE Healthcare) packed with 330mL bed size of Superdex 200 media (GE Healthcare). This type of media has excellent gel filtration properties and is a combination of cross-linked dextran with the physical and chemical stabilities of highly cross-linked agarose. In addition, purification of globular proteins range is from 10,000 to 600,000 Da. Therefore, since our recombinant protein has an estimated molecular weight of 72kD, this form of gel filtration was expected to be ideal for us. We used the previously described AKTA apparatus with the standard gel filtration manufacturers protocol using Gel Filtration Buffer (20mM Tris HCl pH 7.3, 150mM NaCl) (Sigma Aldrich) at a flow rate of 0.5mL/min, a pressure no more than 0.3mPa, and an elution gradient of 1.5 column volumes (495mL).

2.3 Results

2.3.1 Small scale expression of R318 in different protein expression vectors in Origami B cells.

R318 was essentially insoluble when it was expressed alone in pET22b, or as a GST-fusion protein in the cytoplasm of *E. coli*, even at the temperature as low as 15°C. We hypothesize that the disulfide bonds in the Ig domain of R318 play an important role in protein folding and solubility, while the reducing environment of the cytoplasm disfavors formation of the disulfide bonds. The low yield of R318 protein could be attributed to one or more of the factors, such as low efficiency of protein transport from the cytosol to the periplasm, the small space of the periplasm relative to the cytoplasm, and the low efficient disulfide bond formation, etc. To increase the yield of R318, we tested the expression of R318 in the Origami B strain of *E. coli* (**Figure 1**). Origami B strain carries the *trxB/gor* mutations that delete the activities of glutathione reductase and thioredoxin reductase, which greatly enhances disulfide bond formation in the cytoplasm. Moreover, Origami B strain contains characteristics of *lacZY* deletion mutants of *E. coli* BL21 that enable adjustable levels of protein expression by titrating IPTG concentrations. Surprisingly, when induced with 0.1 mM IPTG at 15°C, R318 with either a His-tag (R318-His6) or a GST-tag (GST-R318) was still insoluble (**Figure 1 A and B**). MBP-R318 was expressed in a low level, and the western blot showed that only 10% of MBP-R318 was in soluble faction (**Figure 1C**). After all of the unsuccessful attempts, we cloned the gene encoding R318 into the pCOLD-TF (trigger factor) vector to express a TF-R318 fusion protein under the control of the cspA cold promoter. After induction with 1 mM IPTG at 15°C, the fusion protein was

overexpressed in Origami B cells and the majority of TF-R318 was in soluble fraction (**Figure 1D**).

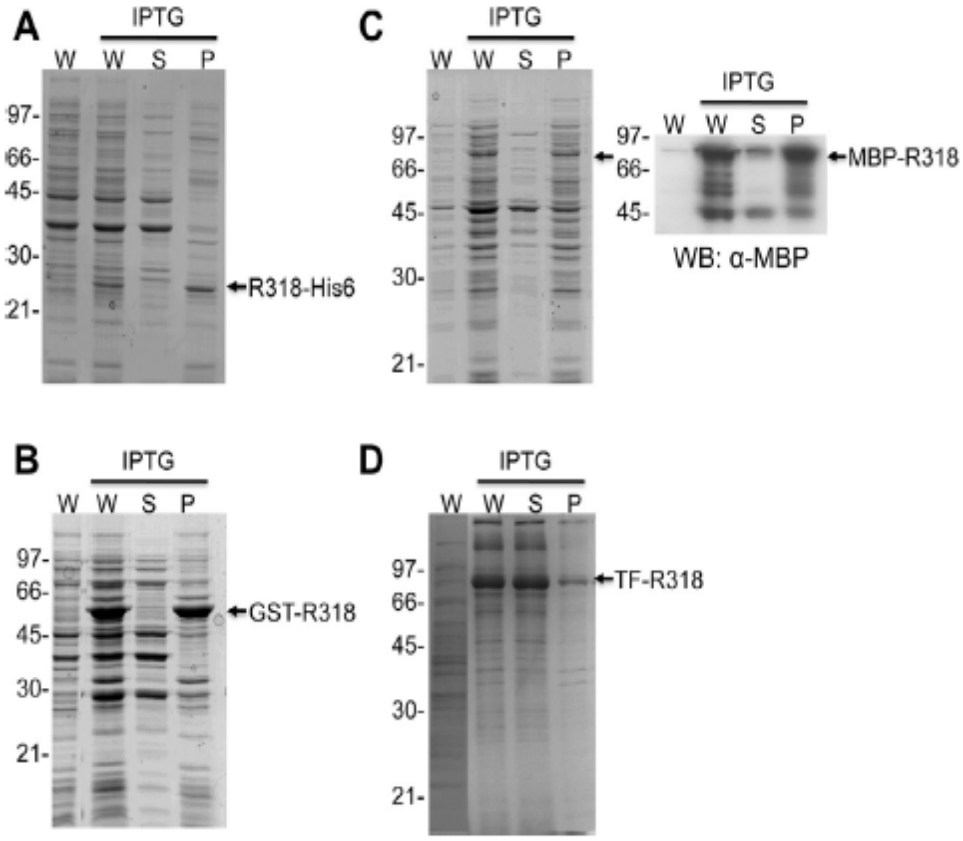

Figure 1. TF-R318 under the control of a cold promoter is expressed as the most soluble protein. R318 with different fusion tags were expressed in Origami B cells as indicated. **A.** R318-His6; **B.** GST-R318; **C.** MBP-R318; **D.** TF-R318. The cells were harvested, lysed and fractionated by centrifugation. The whole cell lysates (W), soluble fraction (S) and insoluble pellet (P) were subjected to SDS-PAGE, followed by Coomassie blue staining. The fusion proteins were marked with arrows. Expression of MBP-R318 was further confirmed by western blot using an HRP-conjugated anti-MBP antibody (**C**).

2.3.2 R318 was purified into homogeneity through a series of chromatography.

The large-scale expression of TF-318 was performed in 4-liters of LB medium, where TF-R318 in Origami B cells was induced at OD_{600} 0.6-1.0 with 1 mM IPTG at 15 °C for 16-24 hours. At such a low temperature, expression of most endogenous proteins was inhibited, but expression of TF-R318 under the control of the cspA cold

promoter was highly activated. At the time of harvest, TF-R318 was account for about ¼ of the total soluble proteins (**Table III** and **Figure 2B**). The soluble lysate was first applied to a nickel column, and the His-tagged TF-R318 was purified by immobilized-metal affinity chromatography (IMAC) (**Figure 2A**). The eluted TF-R318 appeared to be a mixture of soluble oligomeric TF-R318, termed (TF-R318)n, and monomeric TF-R318, which were further separated by a sizing exclusion chromatography using a Superdex 200 column (**Figure 2C**). In SDS-PAGE without the reducing agent, the oligomeric (TF-R318)n was run as a smear with various oligomeric forms, while in the presence of the reducing agent, the majority of the oligomeric (TF-R318)n was reduced and run as a single monomeric band, suggesting that majority of the oligomeric (TF-R318)n was formed by cross-linking of the inter-molecular disulfide bonds (**Inserted figures in Figure 2C**). The monomeric TF-R318 was cleaved by Factor Xα and passed through a nickel column, in which the His-tagged uncut TF-R318 and the free TF were retained in the column and the free R318 was collected in flow through. Finally, the free R318 was purified into homogeneity by a sizing exclusion chromatography using a Superdex 75 column (**Figure 2D**).

Table 3. Summary of Purification of TF R318/R318.

Chromatography	Total protein (mg)	TF-R318/R318 (mg)	Percent yield (%)
Lysate (soluble fraction)	475 ± 25	100 ± 10	100
IMAC (nickel affinity)	60 ± 2	50.2 ± 3	54.2
Sizing exclusion: Superdex 200	10.2 ± 1	10 ± 0.5	10
Sizing exclusion: Superdex 75	5.1 ± 2	5 ± 2	5

The results of this table are estimated from several repeats of purifications. Quantification of the proteins was performed by either using BCA protein assay or densitometric scans of Coomassie-stained bands. In either case, known concentrations of BSA were used as standards.

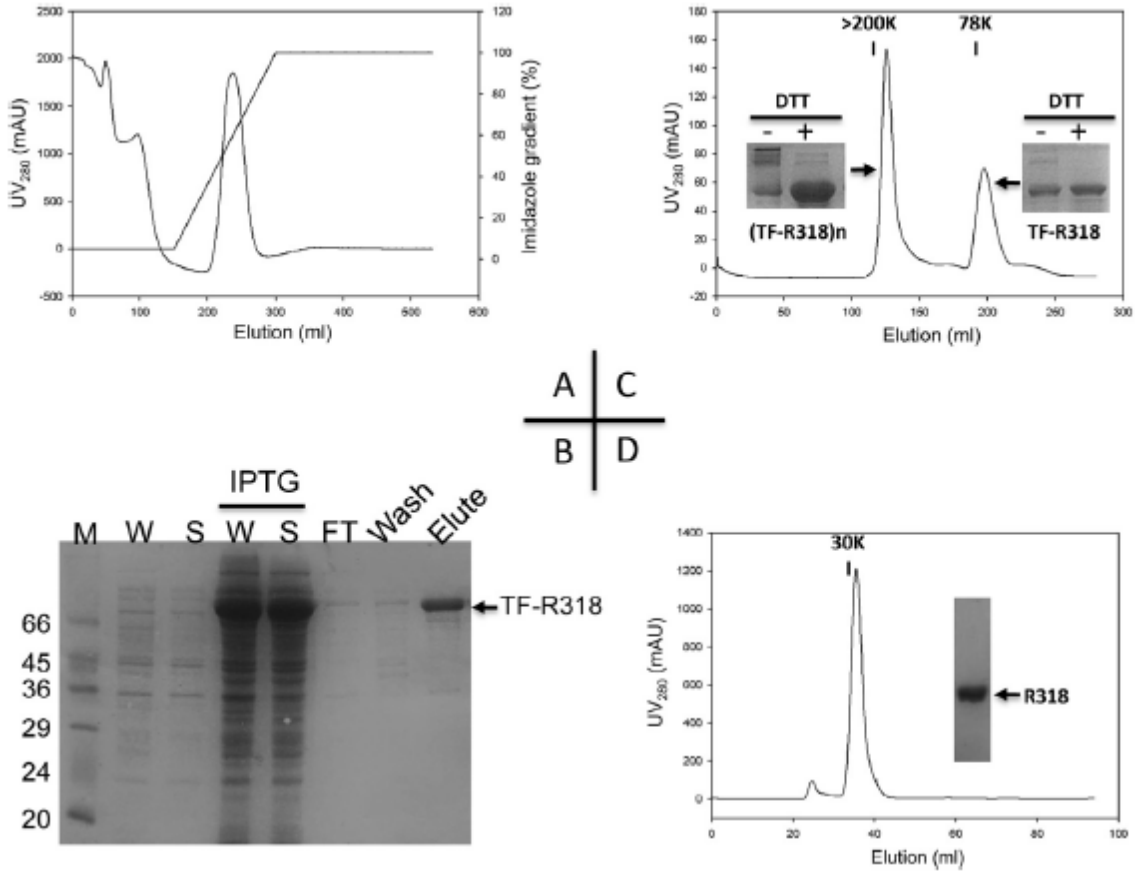

Figure 2. R318 was purified into homogeneity through a series of chromatography. **A.** The N-terminally His-tagged TF-R318 was purified by an immobilized-metal affinity chromatography (IMAC) using a Ni-sepharose column. The soluble fraction of cell lysate containing TF-R318 was applied to a Ni sepharose column, followed by wash and elution with an imidazole gradient in an AKTA FPLC unit. The majority of TF-R318 was eluted at 30-60% of Buffer B containing 500 mM imidazole. **B**. After purification by IMAC, the samples of whole cell lysate (W), supernatant (S), flow through (FT), wash and elute, were collected and applied to SDS-PAGE to analyze the purification efficiency. As a control, the cell lysates (W and S) before IPTG induction were also analyzed to show the IPTG-inducible expression of TF-R318. **C.** The TF-R318 eluted from the Ni-column was concentrated and applied to a Superdex 200 column for sizing exclusion chromatography, in which the soluble oligomeric (TF-R318)n and the monomeric TF-R318 were separated. **Insert Figures:** the oligomeric (TF-R318)n and monomeric TF-R318 were analyzed by SDS-PAGE with or without DTT, followed by Coomarssie blue staining. **D.** The monomeric TF-R318 was incubated with Factor Xα, and then passed through a Ni-column to remove the His-tagged TF. The free R318 was collected in flow through. R318 was further purified by a sizing exclusion chromatography using a Superdex 75 column. R318 was eluted as a ~ 30 kDal monomeric protein and was purified to nearly homogeneity as shown in SDS-PAGE.

2.4 Discussion

The structural and functional analysis of the Ig domain of ANTXR2 is significantly hindered due to the limited production of the recombinant ectodomain, R318. R318 was fused to the bacterial chaperone Trigger Factor, and over-expressed the TF-R318 fusion protein at a low temperature under the control of a cold-shock promoter in the cytoplasm of Origami B cells, where formation of disulfide bonds is favored. This newly developed protocol has significantly increased the solubility of R318 and allowed us purify the functional R318 into homogeneity, which will facilitate biochemical and structural characterization of R318 in future.

When expressed as a GST-tagged protein in *E. coli*, R218 is soluble, but R318 is not soluble, suggesting that the Ig domain play a major role in the folding of the whole ectodomain. The insolubility of R318 in *E. coli* was apparently attributed to the reducing cytoplasm of *E. coli*, where disulfide bond formation is not favored. While the periplasm is regarded as an oxidative environment favoring disulfide bond formation, protein production in the periplasm is usually lower than that in the cytoplasm due to a number of reasons, especially when target protein has a poor solubility and requires expression at a low temperature with a low concentration of IPTG. Thus, Origami B strain that contains a modified oxidative cytoplasm becomes an attractive host for expressing target proteins that contain disulfide bonds. It was surprising that R318-His6, GST-R318 and MBP-R318 were still not soluble when expressed in Origami B cells, even with low IPTG induction and at a low temperature. This strongly suggests that in addition to the disulfide bonds, other factors also play an important role in the folding of R318 in *E. coli*. We have tried co-expression of R318 with the plasmid pG-

KJE8 (Takara) that encodes a set of chaperones (dnaK-dnaJ-grpE-groES-groEL) in Origami B cells, but the solubility of R318 was not improved (data not shown). The observation that fusing R318 to the Trigger Factor significantly increased the solubility of R318 indicates that the TF-mediated co-translational folding of the newly synthesized polypeptide of R318 is the rate-limiting step for producing correctly folded R318 in *E. coli*. It is worthy of mentioning that expression of a His-tagged R318 in the pCOLD vector (with the cspA cold shock promoter, but without TF fusion) did not produce soluble R318 (data not shown). This again strongly suggests that TF is the unique chaperone that is required for correct folding of R318 at the translational step. One can image that in the process of translation, TF mediates the folding of the backbone of the R318 polypeptide and brings the pairs of the Cys residues for disulfide bond formation in the Ig domain to close proximity, allowing formation of the disulfide bonds. And the formation of the disulfide bonds in turn stabilizes the folding of the protein backbones.

Expression of target protein at low temperature is a common approach to increase solubility of target protein in *E. coli*. However, there is a trade-off between solubility and productivity, which has to be carefully balanced. In this study, the trade-off was resolved by application of the cspA cold shock promoter that overly expressed TF-R318 at 16°C, a temperature where expression of the most endogenous proteins was repressed. Thus, TF-R318 was expressed as a dominant soluble protein in the cells, which greatly increased the productivity and facilitated purification.

Chapter 3: Structural Characterization of R318

3.1 Identifying the disulfide bond linkage of R318.

As previously stated, R318 has seven cysteine residues that form three disulfide bonds (23). The specific residues are C39, 175, 218, which are in the VWA-R218 region, and it is well established that C39 and C218 form a disulfide bond meanwhile 175 remains as a free thiol (51). Furthermore, C230, C255, C279, C315, are residues in the Ig-like domain, in which Sun et. al. (23) have reinforced that C175 remains as a free thiol by using Ellman's reagent, and that the six other cysteine residues form three disulfide bonds. In addition, they also concluded that these two disulfide bonds might be important for toxin pore formation once inside the acidic cellular compartment (23). The exact pairing of the four disulfide bonds in the Ig-like domain of R318 remains elusive. In addition, there is no known structural data of R318, which makes it difficult to develop a mechanism to understand toxin action. With that in mind, it is important to map out the disulfide bond linkage in R318, in order to further investigate the role of the disulfide bonds in anthrax toxin action.

3.2 Materials and Methods

3.2.1 R318 Cysteine to Alanine mutants

Cysteines in the Ig-like domain of R318wt were mutated to Alanine residues in pCOLD TF by using Quickchange mutagenesis kit (Agilent Technologies) following manufacturer's protocol. Mutations were confirmed by sequencing. Expression and purification of R318 mutants were done as previously mentioned in R318wt.

3.2.2 Tryptophan fluorescence

5 μM of R218, R318, the C/A mutants of R318 were treated with/without 10 mM TCEP in 20 mM Tris-HCl, 100 mM NaCl, pH 7.3. Emission spectra of Trp59 fluorescence were recorded in an ISS-K2 multiphase frequency and modulation fluorometer from 300-370 nm with excitation at 290 nm. The spectra were calibrated using the same buffers with/without TCEP.

3.3 Results

3.3.1 The residues C255/C279 and C230/C315 form two disulfide bonds in the Ig domain of ANTXR2

To determine the exact disulfide pairing in the Ig domain, we generated a series of mutations by replacing Cys with Ala two at a time in all possible combinations: C230A/C255A, C230A/C279A, C230A/C315A, C255A/C279A, C255A/C315A, C279A/C315A. As a control, we also replaced all of the Cys residues with Ala, which generated the 4C/A mutant. Following the previously described procedures, we expressed and purified the recombinant receptor ectodomains with respective C/A mutations in *E. coli*. While all of the proteins were expressed at a similar level in *E. coli,* only the proteins with mutations C230A/C315A, C255A/C279A and 4C/A were purified as soluble monomeric proteins (**Figure 3B, 3C**). And the rest of the mutants failed to be purified, because they formed aggregations in the cells, which was primarily due to mis-folding and/or disulfide crosslinking. Moreover, a mass spectrometry analysis of the purified R318 recovered 55% of the sequence, in which two trypsin-digested polypeptides were linked by the disulfide bond formed by C255 and C279. Together, this result suggests that C230/C315 and C255/C279 form two stable disulfide bonds in the Ig domain (**Figure 3A**). The disulfide linkage is consistent with the results

in a recent report (53), in which C230/C315 and C255/C279 were predicted to form two disulfide bonds by homologous modeling and by expression of the receptor genes containing C/A mutations in mammalian cells.

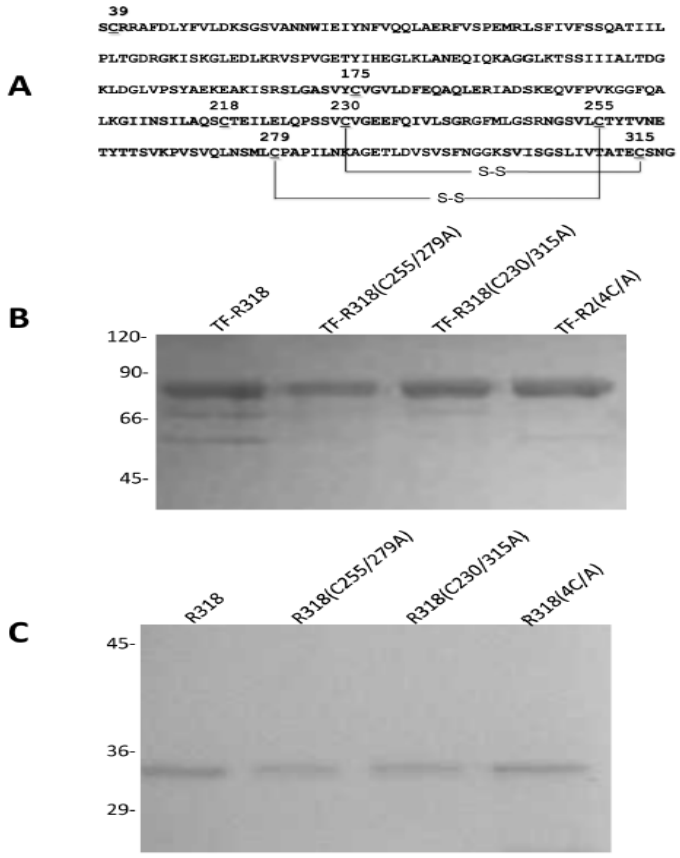

Figure 3. The residues C255/C279 and C230/C315 form two disulfide bonds in the Ig domain of ANTXR2. **A.** Sequence of ANTXR2 showing that C255/C279 and C230/C315 form two disulfide bonds in the Ig domain. **B.** Coomassie blue stained SDS-PAGE of purified TF-R318 and the (C/A) mutants of TF-R318 as indicated. **C.** Coomassie blue stained SDS-PAGE of R318 and the (C/A) mutants, further purified through removal of TF tag.

3.3.2 Reduction or deletion of C255-C279 resulted in a significant conformational change on the receptor ectodomain.

Trp59 is located at the top of VWA domain that is close to the PA binding interface, and it is the only Trp residue in the whole ectodomain. Here, we tested the intrinsic fluorescence of Trp59 to monitor the conformational changes induced by

disulfide disruption. The spectra of Trp59 fluorescence on R218, R318, R318(C230/315A), R318(C255/279A), and R318(4C/A) were measured in the presence or absence of TCEP (**Figure 4**). R218 is not responsive to TCEP treatment, which is consistent with the previous finding that C39-C218 is dispensable for maintaining the VWA structure (49, 51). R318 underwent a significant conformational change upon TCEP treatment, evidenced by a shift of the spectrum peak from 320 nm to 330 nm. R318(C230/315A) displayed spectra that were similar to R318, suggesting that deletion of C230-C315 did not affect the receptor conformation. However, R318(C255/279A) without TCEP treatment has a spectrum peak at 330 nm, and it made no additional conformational change upon TCEP treatment, indicating that deletion or reduction of C255-C279 was responsible for the receptor conformational change. As predicted, R318(4C/A) had a spectrum peak at 330 nm in the presence or absence of TCEP. The result clearly demonstrated that the disulfide bond C255-C279, in either forming or breaking, is responsible for two distinct conformations of the receptor ectodomain, Conformation 1 (C1) with the spectrum peak of Trp59 at 320 nm or Conformation 2 (C2) at 330 nm.

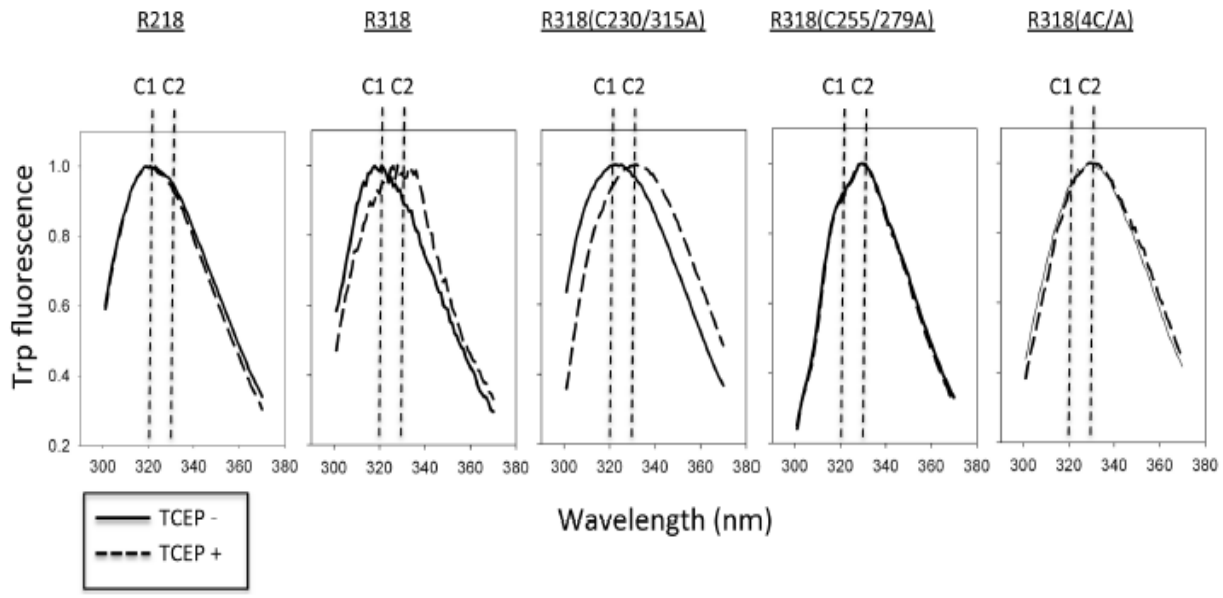

Figure 4. Deletion of C255-C279, but not C230-C315, resulted in a significant conformational change on the receptor ectodomain. 5 μM of the purified receptor domains were incubated in the 20 mM TrisHCl (pH 7.3), 100 mM NaCl, in the presence or absence of 5 μM TCEP. The intrinsic Trp59 fluorescence spectrum was measured with excitation at 290 nm and emission at 300-370 nm. Note: two distinct spectrum peaks (320 nm and 330 nm) were detected and represented as two distinct conformations, denoted as C1 and C2.

3.5 Discussion

In this chapter, we have determined the disulfide bond linkage in R318wt using different R318 cysteine mutants that were created and purified as previously described. We believe that mutation in C230/315A of R318 did not cause a change in conformation in the receptor structure, but mutation in C255/279A of R318 did. This is evidenced by the tryptophan fluorescence study **(Figure 4)**, in which native R318wt and R318(C230/315A) follow the same red shift spectra as both native or disulfide bond reduced VWA. But, R318(C255/279A) and 4C/A could not fulfil this red shift neither in their native nor reduced state. This justifies that the tryptophan in these last two mutants must be more solvent exposed whether the mutants are reduced or not, and

therefore having a similar structure. This also indicates that these reduced forms of R318wt and mutants cause an effect on the VWA structure. We would also like to mention that in addition to this structural data, we collaborated with Dr. Chuan Xiao from the Chemistry Department at the University of Texas at El Paso, in which in silico analysis has indicated that the residues 219-318 form an Ig fold (23, 53), its structure and position in the PA-receptor heptameric complex are still unknown. Using single-particle 3D reconstruction, we determined a low-resolution map (~14Å) of PA-R318 heptameric complex, using negatively stained samples (**Figure 5C, E, G**).

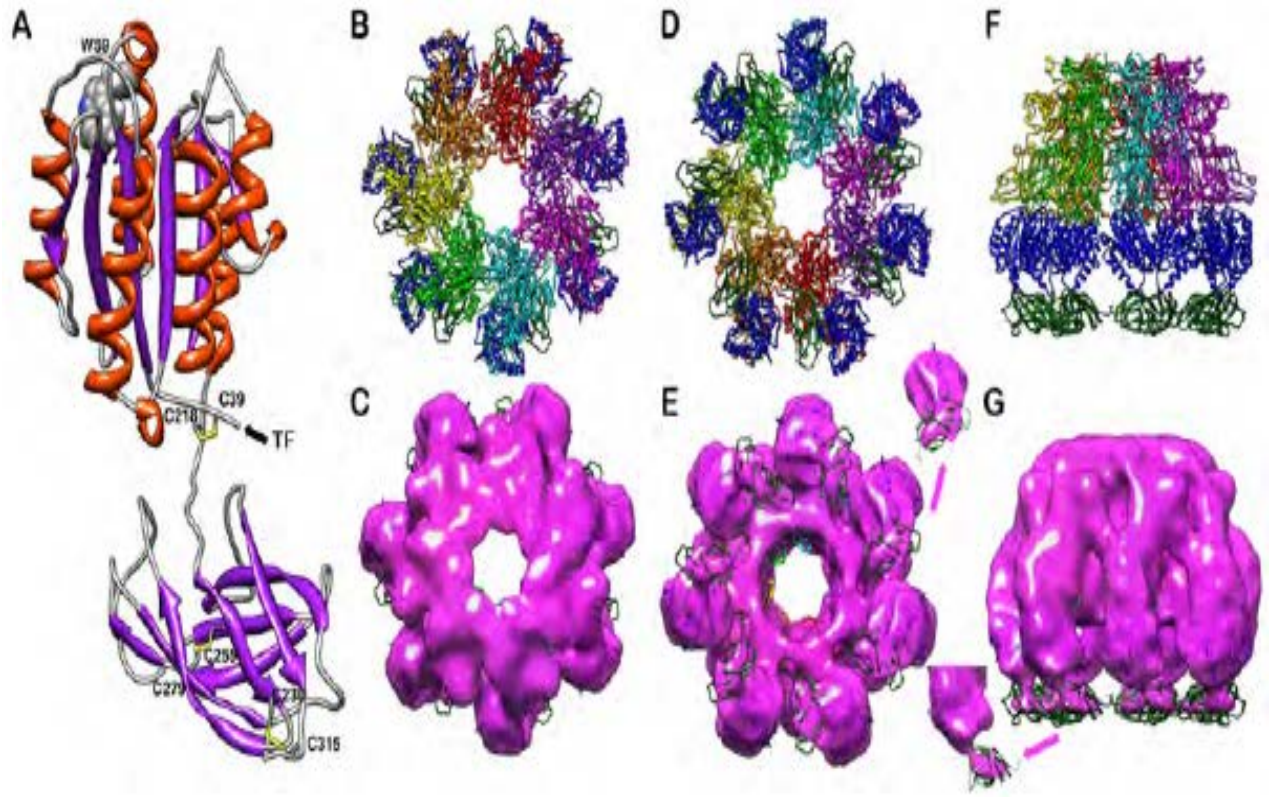

Figure 5. Homology modeling of the Ig domain and docking of the atomic structure into the reconstructed EM maps. A. The structure of the Ig domain is generated by homologous modeling and grafted to the crystal structure of the VWA domain through energy minimization. The secondary structure is colored as α-helices in orange, β-sheets in purple and loops in grey. The disulfide bonds C39-C218, C255-C279 and C230-C315 are shown as stick models, colored in yellow. Note: Trp59 is shown in a sphere model and labeled. **B**, **D**, and **F** are ribbon diagrams of PA-R318 heptameric complex viewed from top, bottom and side, respectively. **C**, **E**, and **G** are surface rendered density maps from reconstruction of negatively stained PA-R318 heptameric

complex, docked with the modeled structure and viewed from top, bottom and side, respectively. Segmented map density of one subunit of the receptor ectodomain is shown on up-right in **E** or lower-left in **G**, respectively. The map was rendered at the level of one standard deviation above the average density value of the map. Within the PA heptamer, each of the seven monomers are colored in red, orange, yellow, green, cyan, magenta, and purple, respectively. The VWA domains and the Ig domains are colored in blue and green, respectively. The reconstructed EM maps are rendered in magenta.

In parallel, we generated a structural model of ANTXR2 ectodomain by homology modeling (**Figure 5A**). The modeled Ig domain in combination with the crystal structure of PA-VWA heptameric complex was docked in the reconstructed EM map (**Figure 5 B-G**). Apparently, the modeled Ig domain fit into the additional density underneath the complex. We also noticed that the density of the Ig domain was significantly weaker than that expected by molecular weight and only appeared when the contour level of the map drop to one standard deviation above the average density level, while the other part of the complex can be rendered at three and half standard deviation above the average density level and still fit the atomic model very well. This suggests that the Ig domain is flexible in solution compared to PA and the VWA domain. This is consistent with the structural model, in which the hinge region between VWA and Ig allows certain flexibility between the two domains. We hope to further obtain high-resolution structural data by crystallography or other methods. This would also help us better understand what other residues in the R318 structure might be affected upon mutation or reduction of the disulfide bonds. Most importantly, it can help us develop a structural mechanism in which reduction of the disulfide bonds in R318 might have upon anthrax toxin action.

Chapter 4: Investigating the role of the disulfide bonds in R318 in anthrax toxicity

4.1 Understanding the influence of the disulfide bonds in R318 towards anthrax toxin action.

Sun et. al have previously described that upon reduction of the disulfide bonds in R318, there is inhibition of pore formation in the toxin/receptor complex in both synthesized lipids and CHO-ANTXR2 cells (23). Yet, it is unknown if the reduction of R318 inhibits the conformational change of the toxin/receptor complex, or if the conformational change occurs as well as the pore formation, but the pore is blocked and there is no toxin translocation. It is not known which of the two processes happen due to the reduction of the receptor. In addition, we also do not know which of the two disulfide bonds in the receptor are crucial for pore formation, or if both are required in order for this step to occur. Preliminary data shows that there might be a correlation between the disulfide bonds in the receptor and the mechanism in toxin translocation in a cellular acidic compartment.

4.2 Materials and Methods

4.2.1 Protective antigen purification and preparation

PA was cloned into pET22b, and then transformed into BL21 (DE3) (NEB) *E. coli* cells using the previously mentioned transformation protocol. They were plated and later grown in a 115 Fermentor/Bioreactor 2.5 liter fermentor (BioFlo/CelliGen). Then the cells were grown at 37°C and when OD_{600} reaches 1, the temperature was lowered to 30°C and induced with 1mM IPTG. The induction time was 4 hours and cells were harvested and lysed by Osmotic Shock (30). Furthermore, PA was then purified by Anion Exchange Chromatography using Buffer A (20mM Tris HCl, pH 8.5) and eluting with Buffer B (20mM Tris HCl, pH 8.5, 1M NaCl) (49).

Next, in order to form PA prepore heptamer (PA_{63}) from wild type (PA_{83}), we digested PA using the protease trypsin at 1:1000 v/v, and incubated the digested

reaction at room temperature for 30 minutes. Finally, for the purification of $(PA_{63})_7$, we purified the digested sample by Anion Exchange Chromatography following the same purification protocol as previously stated (54).

4.2.2 Pyrene fluorescence

PA_{83} carrying the mutation N306C was labeled with pyrene as previously described with labeling efficiency 80–90% (55). The pyrene-labeled PA_{83} protein was treated with trypsin and then purified as $(PA_{63})_7$ heptamer with ion exchange chromatography. The pyrene-labeled $(PA_{63})_7$ was incubated with R218, R318, and the C/A mutants of R318 at pH 8.5 for 30 mins. Conversion of prepore to pore in solution was triggered by addition of 1/10 volume of 1 M sodium acetate (pH 5.0). Pyrene fluorescence emission was recorded at 540 nm with excitation at 342 nm.

4.2.3 Liposome preparation

Liposomes were prepared as previously described (23, 56, 57). Briefly, DOPC was mixed with Ni^{2+}-chelating lipids, DOGs-NTA-Ni (1,2-dioleoyl-sn-glycero-3-{[N(5-amino-1-carboxypentyl) iminodiacetic acid-]succinyl nickel salt}) with a molar ratio 100:8 in chloroform (Avanti Polar Lipids). The lipid was dried under N_2 gas to form a lipid film, followed by vacuum for 3 h to remove residual solvent. The dried lipid film was rehydrated with the buffer containing 50 mM of ANTS and DPX to form multilamellar vesicles and subjected to three freeze-thaw cycles and extrusion through a 200-nm pore size polycarbonate filter (Nucleopore) in a mini extruder (Avanti Polar Lipids). The protocol yielded large unilamellar vesicles with an average diameter of 150–200 nm.

4.2.4 Time-lapse intensity measurement of NBD emission

PA_{83} proteins carrying the mutation G305C or N306C were labeled with IANBD as previously described with labeling efficiency 80–90% (60, 61). Then the NBD-labeled PA_{83} proteins were treated with trypsin and then purified as $(PA_{63})_7$ heptamers. NBD emission of PA pores in the liposomal membranes was measured as previously described (60, 61). Briefly, 0.2 μM of $(PA_{63})_7$ was pre-incubated with 1.4 μM of R218-His_6, R318-His_6, or the C/A mutants at pH 8.5 for 30 mins, and then incubated with the Ni^{2+}-liposomes for another 30 mins. The protein-liposome mixtures were transferred to a cuvette with a stirring bar in the ISS K2 fluorometer. NBD was excited at 488 nm, and emission was recorded at 544 nm. Crossed polarizers on excitation, emission beams, and a 520-nm filter were used to reduce the background scatter. After addition of 1/10 volume of 1 M sodium acetate (pH 5.0) to the cuvette, the shift of NBD label from a polar (solution) to a nonpolar environment (liposomal membrane) was monitored. Rates of NBD emission were calculated in SigmaPlot by fitting the curves to the single exponential equation f=y0+a*[1-exp(-b*x)], in which b is the rate of NBD emission at 544 nm.

4.2.5 ANTS/DPX fluorescence dequenching

The ANTS fluorescence dequenching assay for PA pore formation was developed as previously described (56, 57). Briefly, $(PA_{63})_7$ was pre-incubated with R218-His_6, R318-His_6, and the indicated C/A mutants with a molar ratio of receptor/PA at 3:1 in 20 mM Tris-HCl (pH 8.5), 150 mM NaCl, 1mM $MgCl_2$, at room temperature for 30 mins. Then 100 μl of the liposomes doped with ANTS/DPX were incubated with the protein mixture for an additional 30 mins. The protein/liposome mixture was diluted into 1.3 ml of 20 mM TrisHCl (pH 8.5), 150 mM NaCl, 1 mM $MgCl_2$ with continuous

stirring in the ISS-K2 fluorometer with excitation at 380 nm and emission at 520 nm. After the base line was stabilized, 200 µl of 1M NaAc (pH 5.0) was injected into the cuvette, and the fluorescence signal was monitored in real-time. Crossed polarizers on excitation and emission beams, and a 435-nm long path filter were used to reduce the background scatter.

4.3 Results

4.3.1 Deletion of C255-C279, but not C230-C315, inhibited the PA pore-induced dequenching of ANTS fluorescence.

To measure PA pore function, we recently adopted a sensitive, convenient ANTS/DPX fluorescence dequenching assay as a replacement of the K^+ release assay that was previously established in the laboratory (56, 57). ANTS/DPX, the anion/cation fluorophore/quencher pair, is widely used for membrane leakage. ANTS fluorescence is quenched by DPX inside the liposomes, and it is dequenched upon release into the medium. We have shown that ANTS/DPX fluorescence-dequenching assay faithfully replicated the results obtained from the K^+ release assay (56, 57). Here we used this assay to determine effects of disulfide deletion on functioning of PA pore (**Figure 6**). As expected, PA alone caused a low level of ANTS fluorescence dequenching, which was due to pore formation on the liposomal membranes by a portion of the acidification-converted PA pores through random encounters with the membranes. Compared to PA alone, the PA complexed with either R218 or R318 induced significantly higher fluorescence. The result was consistent with the previous findings that reconstitution of PA to the liposomal membranes through interaction of the His-tags on the receptor domains with the Ni^{2+}-chelating lipids on the liposomal membranes greatly enhanced

PA pore formation (23). However, when PA was bound to disulfide deletion mutants either R318(C255/C279) or R318(4C/A), the dequenching of ANTS fluorescence was drastically inhibited, to a level that is even lower than that of PA alone. Again, this result is consistent with our previous findings, where reduction of R318 by TCEP or DTT inhibited the PA-induced K^+ release (23). Interestingly, deletion of C230/C315 only has a partial effect on dequenching of ANTS fluorescence. Together, this data suggests that the disulfide bond C255/C279 is required for functioning of PA pore.

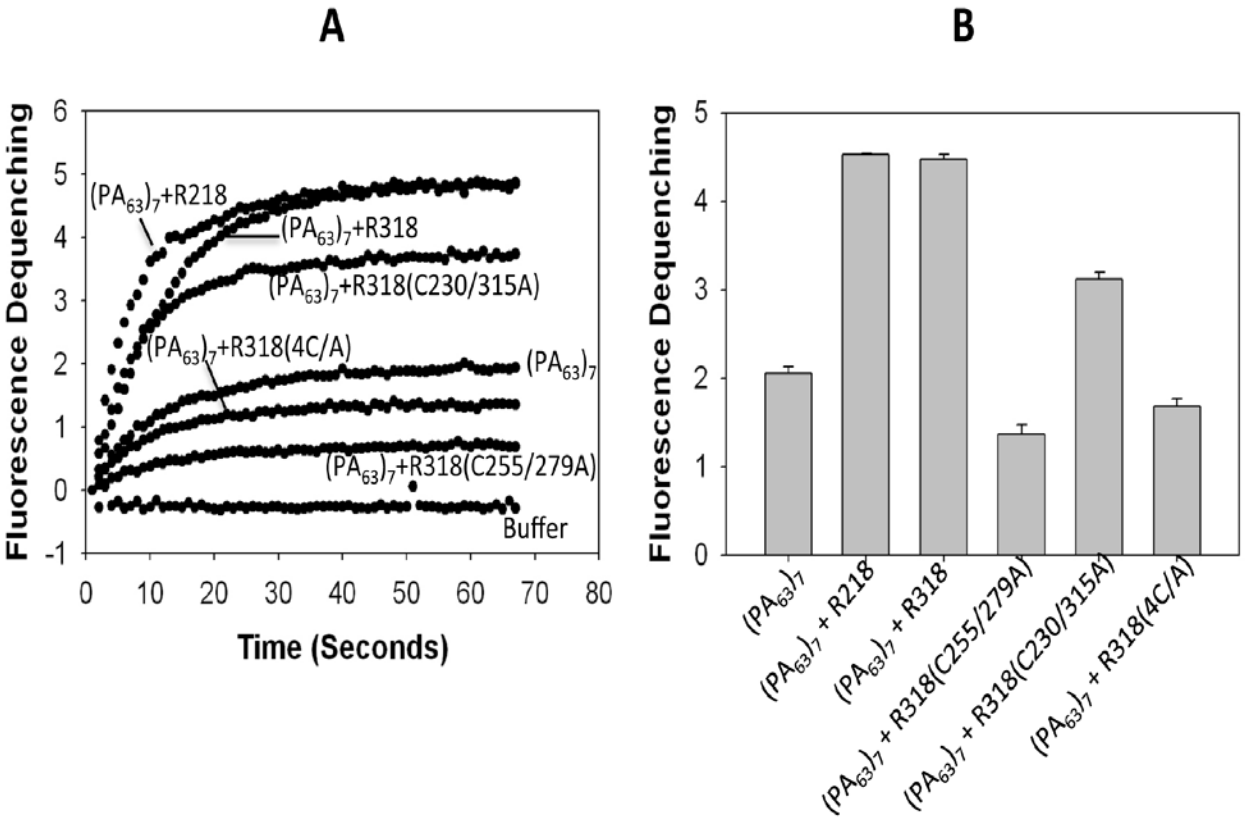

Figure 6. Deletion of C255-C279, but not C230-C315, inhibited the PA pore-induced fluorescence dequenching in the liposomes. The heptameric prepore $(PA_{63})_7$ was bound to the purified receptor domains as indicated, and then incubated with the liposomes doped with ANTS/DPX. Pore formation was triggered by acidification, and ANTS dequenching was measured at 435 nm with excitation at 380 nm. The representative curves of ANTS fluorescence were displayed in **A**; ANTS fluorescence at 60 seconds of post-acidification from three repeats were quantified and shown in **B**.

4.3.2 Disulfide deletion did not affect PA prepore-to-pore conversion.

Next, we sought to test effects of the disulfide deletion on PA prepore-to-pore

conversion. Formation of SDS-resistant oligomers in SDS-PAGE is a well-documented marker for PA prepore-to-pore conversion (55, 62, 63). Previously, we have found that reduction of the receptor by TCEP did not affect PA prepore-to-pore conversion either in solution or on the cell surface membranes (23). Consistent with this result, here we found that deletion of either C255-C279 or C230-C315, or both, did not affect formation of the SDS-resistant oligomer at low pH (**Figure 7A**). To further confirm effects of the disulfide deletion on PA prepore-to-pore conversion, we used pyrene fluorescence to monitor the kinetics of the PA conformational transition in real time. Pyrene is a spatially sensitive extrinsic fluorescent probe, which forms excited-state complexes (excimers) upon close encounter with other pyrene molecules. In a previous study, pyrene maleimide was attached to the residue N306C located on the PA 2β2-2β3 loop. The pyrene labels are too far apart in the prepore structure to interact, but their proximity within the β-barrel of the pore leads to excimer formation and fluorescence (55, 64). Here, we monitored the prepore-to-pore conversion using the pyrene-labeled PA(N306C) that was bound to the receptor domains as indicated (**Figure 7B, C**). Compared to R218 and R318, deletion of either or both of the disulfide bonds in the Ig domain did not exert a significant effect on pyrene fluorescence upon acidification. The result of pyrene fluorescence is consistent with that of the above mentioned SDS-resistant form. In summary, disulfide deletion did not affect PA prepore-to-pore conversion.

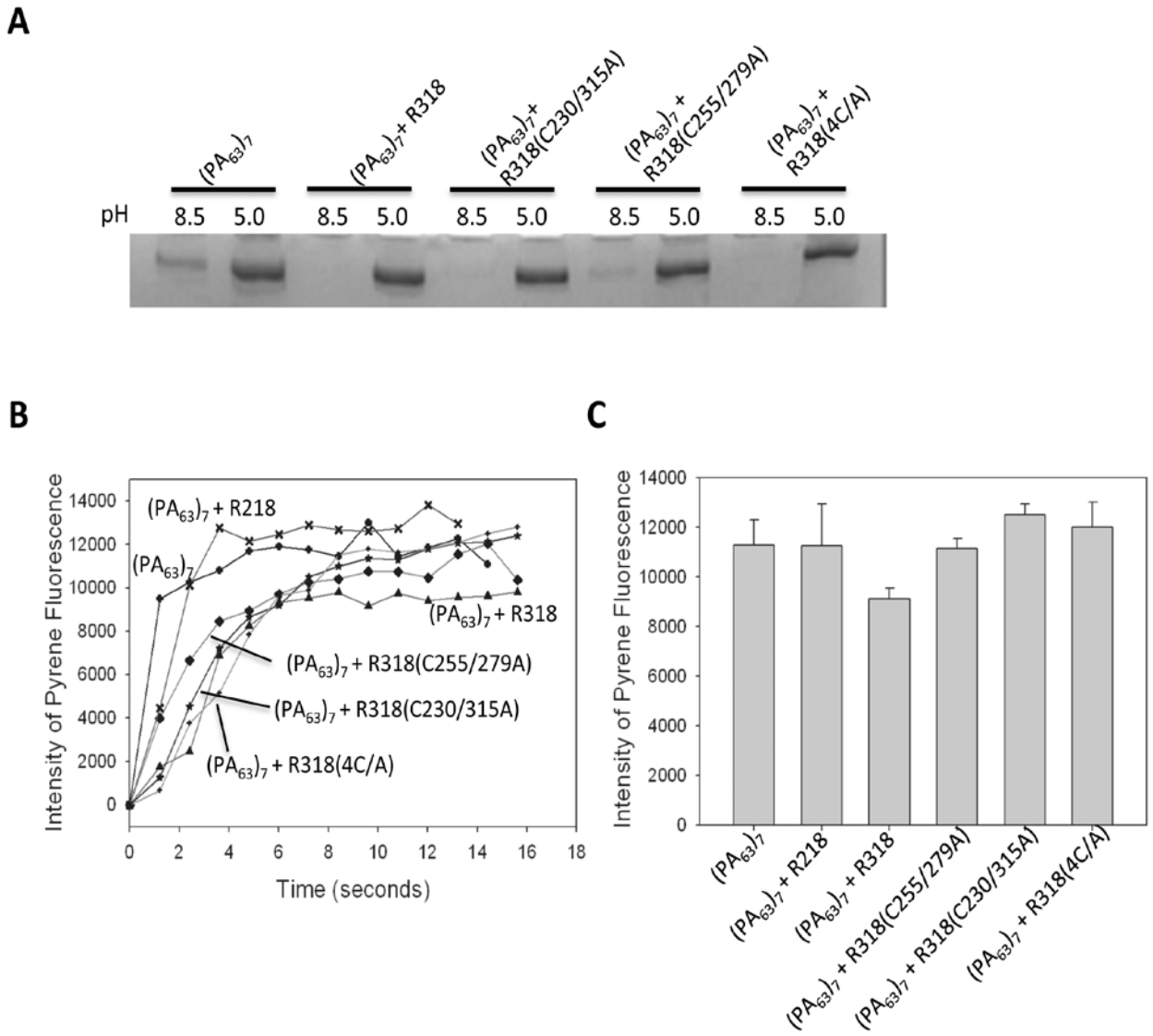

Figure 7. Disulfide deletion did not affect PA prepore-to-pore conversion. **A.** $(PA_{63})_7$ was incubated with the purified receptor domains as indicated in pH 8.5 buffer for 30 minutes in the presence of 1 mM $MgCl_2$. The pH of the buffers either remained constant or dropped to pH 5.0. Subsequently, the formation of SDS-resistant oligomers was examined in SDS-PAGE, followed by Coomassie blue stain. **B**. The pyrene labeled PA(N306C) heptamer was bound to R218, R318 and the R318 C/A mutants as indicated in pH 8.5 buffer. Conversion of prepore to pore was triggered by acidification (pH 5.0) and measured by pyrene fluorescence at 470 nm with excitation at 342 nm. The representative curves of pyrene fluorescence were shown in **B.** The pyrene fluorescence intensity at 15 seconds of post-acidification was quantified and shown in **C.**

4.3.3 Disulfide deletion did affect insertion of PA pore into the membranes.

Since disulfide deletion did not affect PA prepore-to-pore conversion, we tested if it affects PA pore membrane insertion. NBD is an environment-sensitive dye, with

excitation at 488 nm, the emission intensity of NBD fluorescence at 544 nm increases substantially upon a shift from a polar (aqueous) to a non-polar (lipid) environment. Here we used NBD fluorescence to test the effects of disulfide deletion on PA pore insertion on the liposomal membranes. As previously described (60, 61), NBD was attached to the lipid-facing position of PA pore, G305C. As expected, PA alone showed little NBD fluorescence, while the R318-bound PA showed a significantly higher NBD fluorescence. Compared to R318, however, the mutants with deletion of either C255-C279 or C230-C315, or both, produced comparable levels of NBD fluorescence (**Figure 8**). At this point we believed that the disulfide bonds did not have an effect on membrane insertion by PA, until we repeated the assay without liposomes. Unexpectedly, it showed that mutants C255-C279 and 4C/A gave NBD fluorescence even when the liposomes were not present. This proves to us that the NBD molecule inserts into a hydrophobic pocket within the toxin/receptor complex and therefore acting as if it were inserted in the membrane. With this in mind, it justifies that pore insertion is inhibited and that the disulfide bonds impact the membrane pore insertion by PA. As a negative control, we also tested the PA with NBD labeled on N306C, a residue facing the aqueous lumen of the pore. As expected, the NBD-labeled PA(N306C), when bound to R318 or the C/A mutants, did not exhibit any NBD fluorescence (data not shown), indicating that the pattern of PA pore membrane insertion is not affected. Together, the data suggest that disulfide deletion did affect PA pore insertion to the membranes.

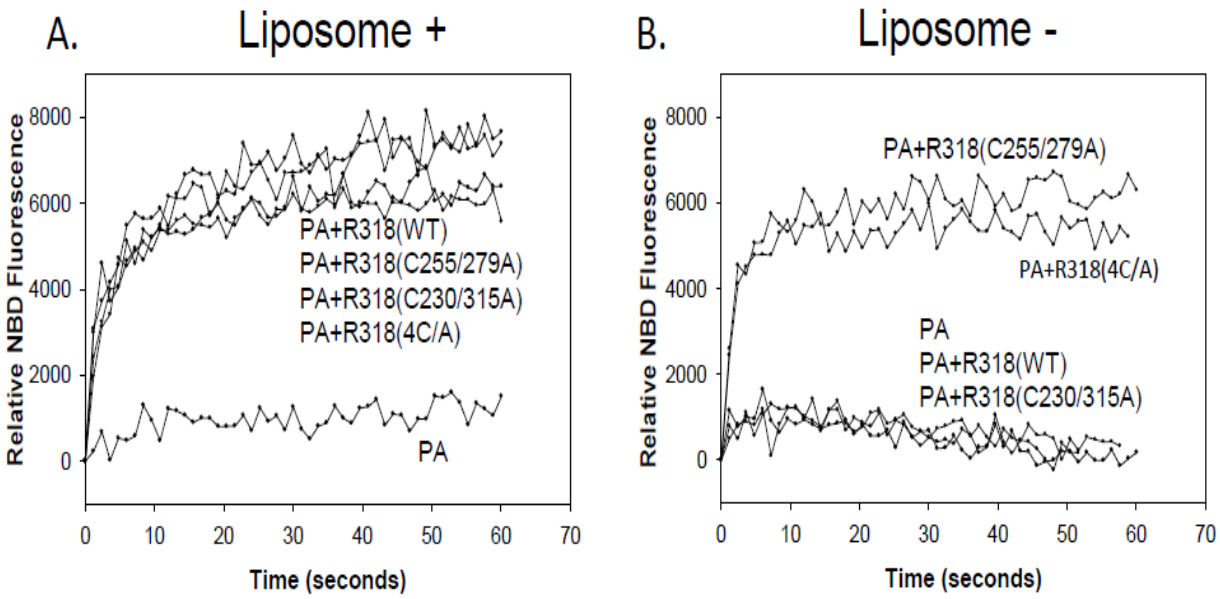

Figure 8. Disulfide deletion did affect membrane insertion of PA pore. The NBD-labeled PA(G305C) heptamer was complexed with the receptor domains as indicated in pH 8.5 buffer. The PA-receptor complexes were pre-bound to the liposomes through binding of the His-tags on the receptor domains to the Ni-chelating lipids on the membranes. Membrane insertion was triggered by acidification (pH 5.0). The NDB fluorescence was measured at 544 nm with excitation at 488 nm. The representative curves of NDB fluorescence were shown in **A**. The curves were fit to the single exponential equation f =ya*[1exp(b*x)], and the rates of NBD.

4.4 Discussion

In summary, we have found that mutant R318C255/279A has an effect on the PA pore forming complex. Initially we believed that this disulfide bonds played a role in blocking the PA pore, based on the ANTS/DPX and potassium release assay, but to our surprise it was not until the NBD assay which helped us understand that this specific bond inhibited the insertion of the PA pore. Therefore, we believe that the disulfide bond mutation does not affect the pore formation and conformational change of PA, but might have an effect on the 14-strand beta barrel inserting into the membrane. More on the collaboration with Dr. Xiao, we observed the conformational changes induced by disulfide disruption, we first reconstructed the EM maps for the heptameric complexes of PA-TF-R318 and PA-TF-R318(4C/A) (**Figure 9A-F**).

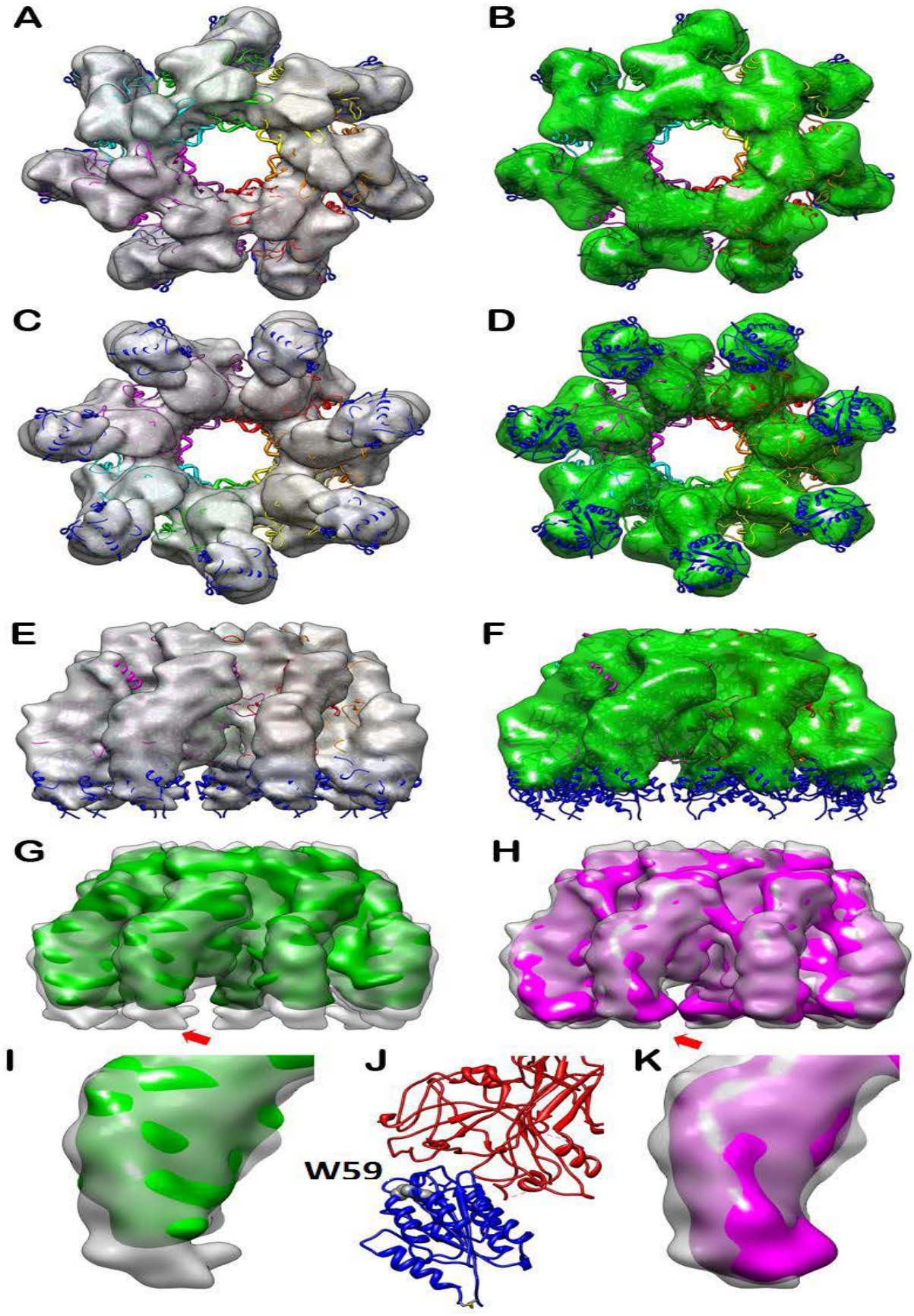
A
B
C
D
E
F
G
H
I
J
W59
K

Figure 9. **3D reconstruction of negatively stained PA-TF-R318 and PA-TF-R318(4C/A) detected the disulfide deletion-induced conformational changes on the VWA domain**. **A**, **C**, and **E** are surface rendered density maps of PA-TF-R318 heptameric complex viewed from top, bottom and side. **B**, **D**, and **F** are surface rendered density maps of PA-TF-R318(4C/A) viewed from top, bottom and side. The crystal structure of the PA-VWA heptameric complex was docked in the reconstructed maps. **G** is the side view of the superposed density maps from PA-TF-R318 (transparent grey) and PA-TF-R318(4C/A) (solid green). **H** is the side view of the superposed density map from PA-TF-R318 (transparent grey) and PA-R318 (solid magenta) showing no significant difference. **I** and **K** are the zoom-in monomeric view for the area at the lower part of the complexes as show in **G** and **H** respectively. **J** is the ribbon diagram of the fitted PA and VWA structure at the same orientation and magnification as in **I** and **K**. All of the maps were rendered at the level of three and half times standard deviation above the average density value of the maps. The PA is colored in red and the VWA is colored in blue. Trp59 of VWA is rendered as spherical model and labeled.

We have described how Trigger factor has improved the solubility and stability of R318 proteins, especially for the R318 Cys/Ala mutants (57). Moreover, TF tag at the N-terminus of R318 did not affect the function of the receptor in mediating PA pore formation (data not shown). More importantly, TF tags appeared to increase the visibility and orientations of the protein particles on the EM grids after negative staining. Surprisingly, however, in the reconstructed EM map of PA-TF-R318 we could not locate the density of Ig domains and TF tags (**Figure 9A, C, E**). We noticed that in the pCOLD-TF vector there is an extended polypeptide linker (26 residues in total) between TF and the inserted gene. This long linker may cause significant flexibility between TF and receptor, which made density mapping of the structures beneath the VWA domains difficult, especially when the maps were rendered at a low contour level. Nevertheless, we rendered the map of PA-TF-R318 at a density level of three and half standard deviation above the average value to remove the disordered density beneath the VWA domains. The resultant map of PA-TF-R318 fits the crystal structure of the PA-VWA heptamer very well (**Figure 9A, C, E**). Using the same parameters, we reconstructed the EM map of PA-TF-R318(4C/A) (**Figure 9B, D, E**). Compared to the map of PA-TF-

R318, PA-TF-R318(4C/A) apparently has less density in the VWA domain (**Figure 9G, I** and **J**), suggesting that the VWA domain on the 4C/A mutant was either partially unfolded and/or became more flexible. This observation is consistent with the data from Trp59 fluorescence experiment. To rule out the possibility that TF tags may interfere with the density mapping, we compared the reconstructed maps of PA-R318 and PA-TF-R318 by superimposing the two maps rendered at a three and half standard deviation above average density level (**Figure 9H and K**). The superimposed map shows that there is no significant difference between two maps, suggesting that the presence of the flexible TF tags did not affect the density mapping of PA and VWA.

Chapter 5: The importance of the disulfide bonds in both R318 folding and anthrax toxicity.

Our study began by taking into consideration the importance of redox reactions in cell surface receptors and their ability to internalize extracellular content into the cell. These redox reactions serve as on and off switches within cell surface receptors in either inhibiting or activating this cellular process. Disulfide bonds serve as a form of these specific switches. With this in mind, we believed that the disulfide bonds in R318 might play a role in the cellular mechanism of internalizing the anthrax toxins into the cell. Before this study, it was believed that R318 formed three disulfide bonds out of seven cysteine residues **Figure 3A** (23). The exact mapping or orientations of these disulfide bonds were unknown. More importantly though was the fact that upon reduction of these disulfide bonds, anthrax toxin pore was blocked in lipid membranes, toxin translocation was inhibited across mammalian cells (23). At this point we believed that in fact R318 was one of these cell surface receptors that have a role in

these redox reactions, and that the disulfide bonds in R318 might be important for anthrax toxicity. But before we continued into further characterizing the disulfide bonds in this receptor and understanding their role with anthrax toxicity, we encountered the challenge of producing fully soluble and functional R318 protein. Expressing and purifying R318 in a bacterial host has become one of the most difficult tasks in this study. This is due to the fact that R318 forms disulfide bond cross-linking between different R318 monomers which leads to oligomerization of the product **Figure 2C**. Furthermore, it is important to address that not only is this the reason why R318 becomes insoluble, but also because the protein does not become properly folded inside the host cell. That is, that even upon treating the oligomers with reducing agent the oligomers a fraction of the oligomers still remains (data not shown). This phenomenon was not further investigated but we believe that it might have to do with some type of hydrophobic interaction between oligomers. We also learned that the receptor is very dynamic and that it can go into redox reactions if its environment is neglected which makes it very unstable. Although it was difficult in overcoming the challenges brought to us in isolating this receptor, both the Origami B strain and the pCOLD vector worked for us successfully. We believe that the Trigger Factor aided as a chaperon in the proper folding and also disulfide bond linkage, and that the Origami strain provided the exact redox environment inside the cell in favor of the receptor. In addition, these two variables also produce fully functional soluble receptor. At this point, we were ready to continue with our structural and biochemical receptor studies.

Our next interest in this study was to map out and characterize the disulfide bonds in R318. As previously mentioned, we only had to determine the formation of the

disulfide bonds in the Ig-domain of R318, since one disulfide bond (C39/218) is formed in the VWA domain of the receptor and residue C175 remains as a free thiol (23). Therefore we wanted to create these different cysteine mutants in order to not only identify the proper formation of these disulfide bonds, but also to test their functionality in regards to anthrax toxicity. Although we were able to create the different mutant DNA constructs, only three receptor mutants were purified including the 4C/A mutant **Figure 3B and C**. Because of the nature of the receptor in proper folding and solubility, we began to believe that these two mutants followed the proper disulfide bond linkage in R318. One reason was the fact that we could not purify the others since they all became misfolded proteins inside the host cell (data not shown). So in order to confirm this hypothesis we decided to do Homolog Remodeling on R318 **Figure 5A**. As predicted, the VWA follows the known homologous I domain of integrin receptors composed of a Rossmann-like α/β-fold in which beta-sheets are surrounded by alpha helices, and a metal-ion-dependent adhesion site (MIDAS) motif on the upper surface. Furthermore, the Ig-like domain is composed of antiparallel beta-sheets and is much smaller than the VWA domain. In addition, this structure also gave the predicted disulfide bond pattern between residues C39/218, C230/315 and C255/279. Further structural characterization lead to the EM reconstruction of the PA heptamer and R318 in both ribbon and density maps **Figure 5B-G**. This specific structure was overlaid with the known PA-VWA complex and proved that the Ig domain is weaker and more solvent exposed in this complex **Figure 5E and G**. Nonetheless, this structure helps us understand where in the complex does the Ig domain rest and how it is incorporated as well. Once we had discovered the disulfide bond mapping and structural

characterization of the PA heptamer and R318 complex, we decide to further study the role of the disulfide bonds in the Ig domain. Before we began our biochemical studies, we decided to test if there are any changes in conformation in the receptor if any of the disulfide bonds were missing, or both. We have described earlier that there is a Tryptophan residues at position 59 in the VWA, and is can be used to measure conformational changes in proteins based in its exposure to the environment. We saw that R318 had two distinct conformations based on its absorption spectra. Both R318 wild type and mutant C230/315 had the same absorption spectra in their native form, but changed similarly when they became reduced. On the other hand, R318 mutants C255/279 and 4C/A had the same absorption spectra in both native and reduced forms. This means that W59 will become more solvent exposed upon reduction of R318 wild type and the C230/315 mutant but is more embedded in their native state. Whereas it is always more solvent exposed in the other two mutants in both native and reduced forms, suggesting that there is a change in receptor conformation upon deletion of residues C255/279 in R318. This type of structural data has not been investigated in depth before and has brought us great insights into the structure and orientation of the Ig domain in R318 which is an important aspect of this study. More importantly though is the fact of the role of the disulfide bonds in anthrax toxin action.

As previously mentioned, if the disulfide bonds in R318 are reduced chemically, anthrax toxin action is inhibited (23). Therefore a very important goal of this project was to identify not only which disulfide bond is responsible, but also at which step is the toxin action inhibited. Ultimately, we hoped to build a possible inhibition mechanism by answering these two questions. So our initial study began by identifying which

disulfide bond in R318 was responsible in blocking the anthrax toxin pore **Figure 6**. Here we saw that mutant C255/279 had a severe reduction in fluorescence signal than the C230/315 and even more surprisingly the C4/A mutant. At this point we realized that not only does the C255/279 mutant cause a noticeable conformational change in the receptor structure, but also that it has the ability to block the anthrax toxin pore in some way. At this point we believed that this mutant actually simply blocked the anthrax toxin pore and could serve as a possible pore inhibitor of the toxin. In order to fully elucidate other possibilities of this mutant in anthrax toxin action, we decided to break down the important step in anthrax toxin action. At this point we knew that both the wild type and mutant receptors binded to PAwt and the PA heptamer. And that they had an effect on the PA heptamer pore action in the leakage assay **Figure 6**. So continuing on, we wondered if it had an effect on the conformational change of the PA heptamer in the pre-pore to pore conversion. To investigate this in a sensitive and efficient manner, we decided to use a fluorescent probe that can measure conformational changes in proteins as well as distances or proximities from one another; this probe is Pyrene (65). Pyrene has the ability to form excimers upon coming to proximity with another molecule of its kind, so if a pyrene molecule becomes excited, it will transmit its excitation to another pyrene molecule if it encounters it but maintains its excited state (65). Another important fact is that the emission spectra of the monomer and excimer pyrenes do not overlap (65). Since it has already been established that the PA pore is approximately 12A˚ (64), pyrene can transmit fluorescence under this proximity. With this said, we labeled N306 with pyrene, which is a residue facing the lumen of the pore, and tested for excimer formation upon pore

formation. This can be achieved since the PA pore will have a total of seven pyrenes in the complex and will give excimer emission if they come in proximity to one another. Surprisingly, we found that all PA-receptor wild type and mutant complexes were able to emit pyrene fluorescence including the PA complex alone. This proved to us that the C255/279 still did not cause an effect in blocking the conformational change of the PA pore. At this point we analyzed the fact that this mutant blocked the PA pore and not its conformational change, but what if it inhibited the pore to be inserted into the lipid membrane. For this approach we used NBD which is a fluorescent probe used as a reported to measure hydrophobic environments (61, 65). Here NBD will emit if it is transitioned from a polar to a nonpolar environment (61, 65). This is a very special phenomenon known as red-shift excitation and is described as molecule orientation in this case NDB. So, in polar solution NBD will form hydrogen bonds in solution but those bonds are broken when the molecule goes into a hydrophobic environment, but this point the molecule becomes relaxed and is able to emit (65). So like the labeling of N306 in the pore lumen, we decided to label a residue in the PA pore, facing the lipid membrane. G305 is a residue that faces the lipid membrane upon pore insertion and can be used to measure this transition (61). Just like the pyrene assay, we noticed that all toxin-receptor wild type and mutant complexes gave a positive emission suggesting that the PA pore is inserted into the membrane. At this point we believed that the C255/279 mutant had only an effect in blocking the PA pore. To our surprise we repeated the assay without lipids and saw a total different result. We saw that both the mutants C255/279 and 4C/A still gave positive emission. So we thought if there aren't any lipids in our assay, and NBD is dependent of a hydrophobic environment,

how could we still obtain a positive signal? For this explanation we had to develop a hypothesis based on our structural data. We believe that if the disulfide bond formed between residues C255/279 is deleted, this causes an effect on the VWA domain of R318 by making it loose density and becoming more solvent exposed **Figure 10**.

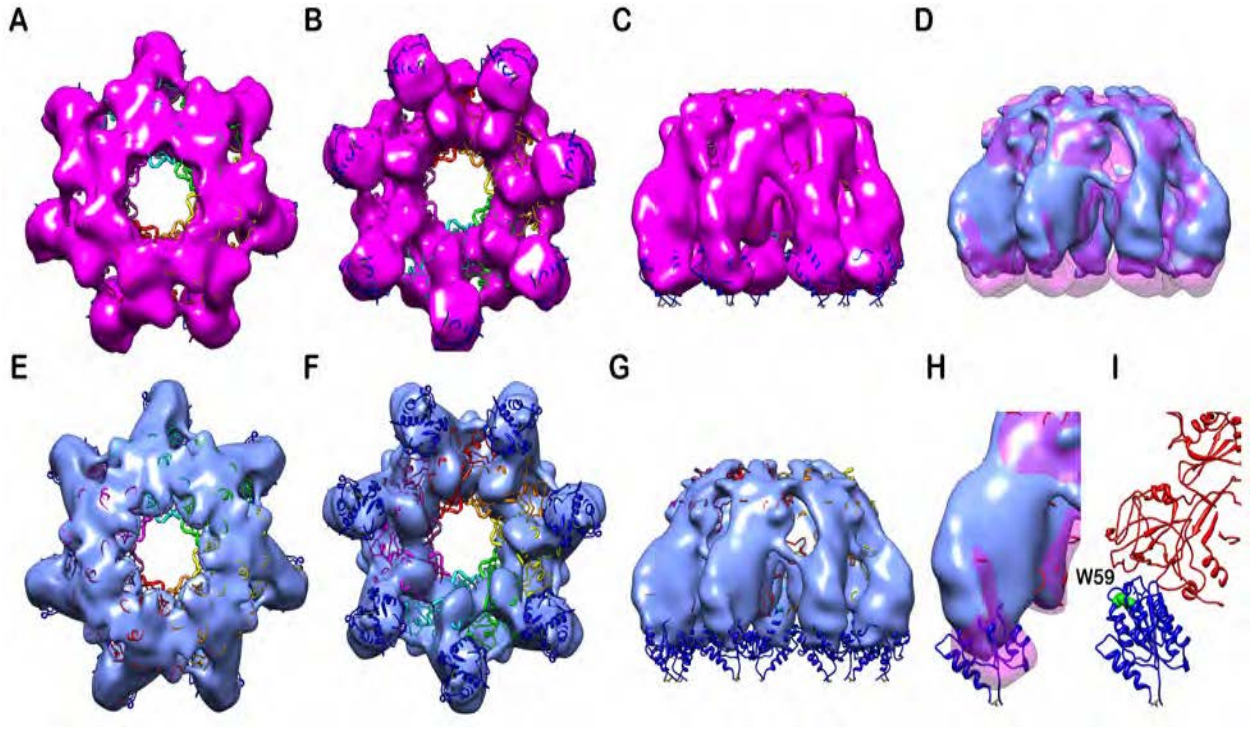

Figure 10: Compared to PA-R318, PA-R318(C255/279A) exhibited a significant conformational change on the VWA domain. **A**, **B**, and **C** are surface rendered density maps of PA-R318 heptameric complex viewed from top, bottom and side in magenta. **E**, **F**, and **G** are surface rendered density maps of PA-R318(C255/279A) viewed from top, bottom and side in cyan. The crystal structure of the PA-VWA heptameric complex was docked in the reconstructed maps. **D** is the side view of the superposed density maps from PA-R318 (transparent magenta) and PA-R318(C255/279A) (solid cyan). **H** is the side view of the superposed density map from PA-R318 (transparent magenta) and PA-R318(C255/279A) (solid cyan) that shows the missing densities in the VWA domain. **I** is the ribbon diagram of crystal structure of PA-VWA heptamer at the same orientation and magnification as in **H**. All of the maps were rendered at the level of three and half times standard deviation above the average density value of the maps. The PA is colored in red and the VWA is colored in blue. Trp59 of VWA is rendered as spherical model and labeled.

Figures 9 and 10 are EM reconstruction maps of PA heptamer and R318 4C/A and R318 (C255/279A) respectively, have helped us understand the importance of the C255/279 disulfide bond in the structure of R318. Taking into consideration that both

of these mutants have this specific disulfide bond mutated you can see how part of the VWA domain R318 becomes more solvent exposed in the PA-receptor complex **Figure 9C-F and Figure 10B-G**. This specific conformational change in the receptor structure has given us reason to believe that it might not allow the PA pore to fully assemble properly and become stable, and therefore not insert into the membrane. The 2β-3β sheets in domain 2 of each of the PA monomers that form the pre-pore complex, move towards the bottom of the PA-receptor complex and form the known 14-beta barrel pore. We believe that the flexibility and relaxation of the VWA domain in these mutants cause an effect on these domain 2 beta sheets to not let it assemble or insert properly. Furthermore, we also believe that they might embed within the R318 structure at the base of the PA-receptor complex, which gave a hydrophobic environment to the beta sheets therefore testing positive for NBD fluorescence. In other words, the beta sheets are going into a hydrophobic pocket provided by the toxin-receptor complex. Our predicted model (**Illustration 6**) suggests that once the PA prepore monomer is bound to an R318 monomer through domain 4 of PA and the VWA in R318, and the conformational change occurs upon acidification, domain 2 moves towards the bottom of the complex and becomes β-barrel stem which gets inserted into the lipid membrane. At the same time domain 1 which is responsible for EF and LF binding, domain 3 in PA oligomerization and domain 4, form a cap at the upper face of the complex (31).

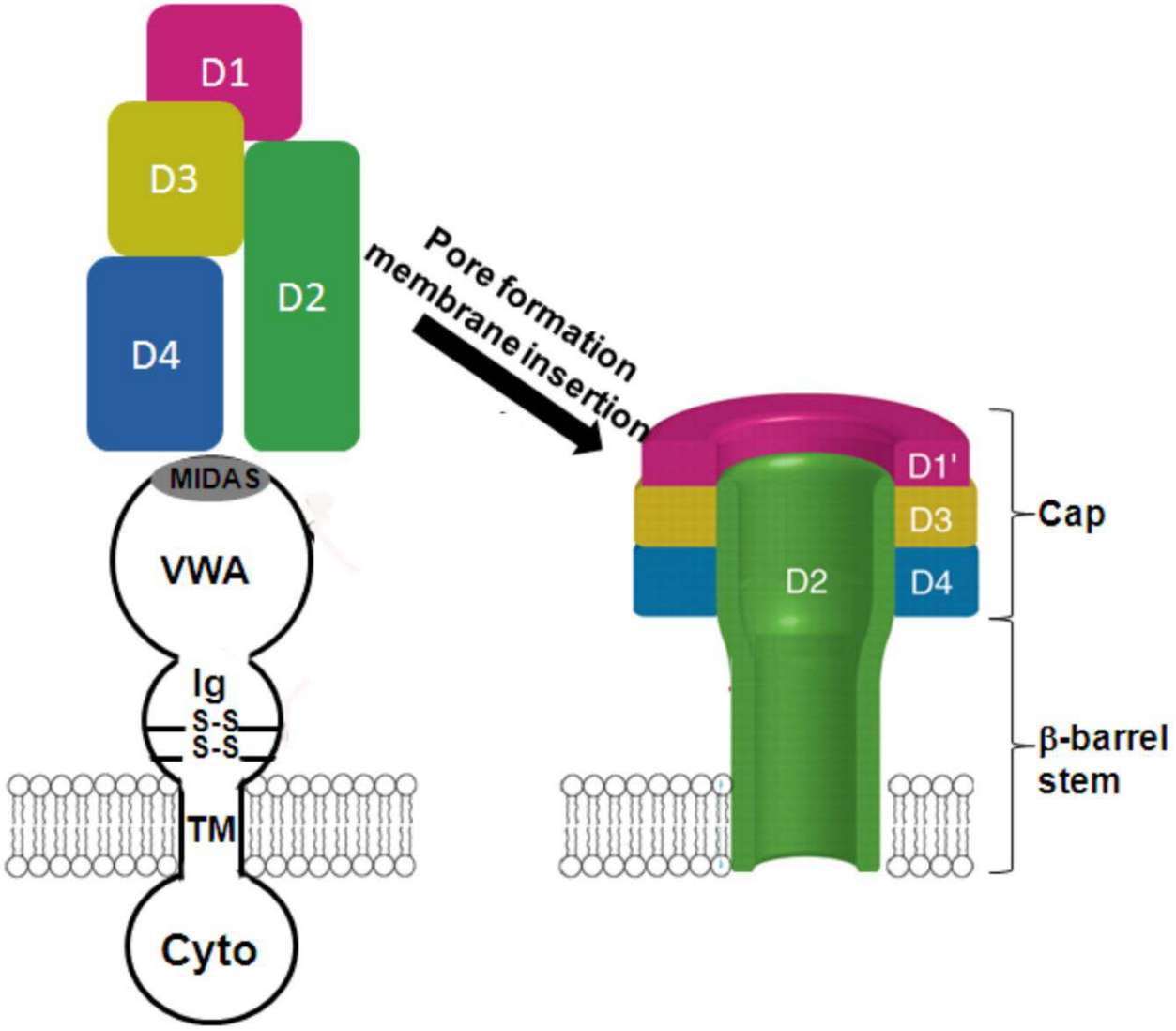

Illustration 6. The classical anthrax toxin model for membrane insertion.

Although this is the classical way in which anthrax toxin takes action, the disruption of the disulfide bonds in the Ig domain of R318 inhibits this transition of domain 2 in PA to insert into the lipid membrane. The exact mechanism for this is still unknown to us but both our structural and biochemical data presented here in this study suggests it.

In a future study we hope to obtain further structural data that can help us exactly identify what is happening to domain 2 of PA upon reduction or deletion of the disulfide bonds in the Ig domain of R318. We are very much interested in knowing exactly

where the beta sheets of domain 2 are imbedded within the R318 structure that do not allow it to fully assemble into its pore shape. In addition to this, we also would want to identify important residues in the beta sheets of PA or R318 in proper pore formation and insertion. Future methods we expect to conduct are either crystallography or electron microscopy as stated in this study. An overall future direction would be to obtain a structure of the entire complex pore which has never been found. This would definitely aid in understanding in depth the mechanism that is caused by the deletion of the disulfide bonds in R318. It would also show us exactly how the pre-mature pore is assembled once these bonds are deleted. More important is the fact that we would like to know how the beta sheets in domain 2 of PA are imbedded prematurely in the proteinaceous hydrophobic pockets. This has brought great interest into our study. This report has brought us great insights in understanding an important role of R318 in anthrax toxicity and that it must be present in order for toxicity to take effect. In addition, the disulfide bonds in the Ig domain of R318 are highly important in allowing the entire toxicity mechanism to take place. We also found important structures that aid in the change in conformation in the receptor if these disulfide bonds are absent. We would like to add that these specific structures have never been identified. We also found that upon deletion of the disulfide bonds in R318 causes aberrant effects on the anthrax toxin by not letting it get inserted into the membrane. With this we hope to continue our research to find better ways to understand anthrax toxicity and therapeutics to it.

References

1. Leppla, , K. Aktories and I. Just, eds., S.H. (2000) Anthrax Toxin in Bacterial Protein Toxins (Berlin: Springer), pp. 445–472.

2. Spencer, RC (March 2003). "Bacillus anthracis.". *Journal of clinical pathology* **56** (3): 182–7. doi:10.1136/jcp.56.3.182. PMC 1769905. PMID 12610093.

3. Holt, J. G., N. R. Krieg, P. H. A. Sneath, J. T. Staley, and S. T. Williams. 1994. Group 17: gram-positive cocci, p. 527–558. In W. R. Hensyl (ed.), Bergey's manual of determinative bacteriology, 9th ed. Williams and Wilkins, Baltimore, Md.

4. Bergey's Manual of Systematic Bacteriology, vol. 2, p. 1105, 1986, Sneath, P.H.A.; Mair, N.S.; Sharpe, M.E.; Holt, J.G. (eds.); Williams & Wilkins, Baltimore, Maryland, USA

5. Zilinskas, Raymond A. (1999), "Iraq's Biological Warfare Program: The Past as Future?", Chapter 8 in: Lederberg, Joshua (editor), *Biological Weapons: Limiting the Threat* (1999), The MIT Press, pp 137-158.

6. National Center for Emerging and Zoonotic Infectious Diseases (NCEZID) 2013. Centers for Disease Control and Prevention. Accessed October 28, 2014. <http:// http://www.cdc.gov/anthrax/types/>

7. National Center for Emerging and Zoonotic Infectious Diseases (NCEZID) 2013. Centers for Disease Control and Prevention. Accessed October 28, 2014. <http:// http://www.cdc.gov/anthrax/types/inhalation.html>

8. Barnes JM (1947). "Penicillin and *B. anthracis*". *J Path Bacteriol* **194**: 113–125. doi:10.1002/path.1700590113.

9. Read, TD; Peterson, SN; Tourasse, N; Baillie, LW; Paulsen, IT; Nelson, KE; Tettelin, H; Fouts, DE; Eisen, JA; Gill, SR; Holtzapple, EK; Okstad, OA; Helgason, E; Rilstone, J; Wu, M; Kolonay, JF; Beanan, MJ; Dodson, RJ; Brinkac, LM; Gwinn, M; DeBoy, RT; Madpu, R; Daugherty, SC; Durkin, AS; Haft, DH; Nelson, WC; Peterson, JD; Pop, M; Khouri, HM; Radune, D; Benton, JL; Mahamoud, Y; Jiang, L; Hance, IR; Weidman, JF; Berry, KJ; Plaut, RD; Wolf, AM; Watkins, KL; Nierman, WC; Hazen, A; Cline, R; Redmond, C; Thwaite, JE; White, O; Salzberg, SL; Thomason, B; Friedlander, AM; Koehler, TM; Hanna, PC; Kolstø, AB; Fraser, CM (May 1, 2003). "The genome sequence of Bacillus anthracis Ames and comparison to closely related bacteria.". *Nature* **423** (6935): 81–6. doi:10.1038/nature01586. PMID 12721629.

10. Kolstø, Anne-Brit; Tourasse, Nicolas J.; Økstad, Ole Andreas (1 October 2009). "What Sets Apart from Other Species?". *Annual Review of Microbiology* **63** (1): 451–476. doi:10.1146/annurev.micro.091208.073255.

11. Mock M, Fouet A. 2001. Anthrax Annu. Rev. Microbiol. 55:647–71

12. Okinaka RT, Cloud K, Hampton O, Hoffmaster AR, Hill KK, et al. 1999. Sequence and organization of pXO1, the large Bacillus anthracis plasmid harboring the anthrax toxin genes. J. Bacteriol. 181:6509–15

13. Dai Z, Sirard JC, Mock M, Koehler TM. 1995. The atxA gene product activates transcription of the anthrax toxin genes and is essential for virulence. Mol. Microbiol. 16:1171–81

14. Fouet A, Mock M. 2006. Regulatory networks for virulence and persistence of Bacillus anthracis. Curr. Opin. Microbiol.9:160–66

15. Koehler TM, Dai Z, Kaufman-Yarbray M. 1994. Regulation of the Bacillus anthracis

protective antigen gene: CO2 and a trans-acting element activate transcription from one of two promoters. J. Bacteriol. 176:586–95

16. Mignot T, Mock M, Fouet A. 2003. A plasmid-encoded regulator couples the synthesis of toxins and surface structures in Bacillus anthracis. Mol. Microbiol. 47:917–27

17. Uchida I, Hornung JM, Thorne CB, Klimpel KR, Leppla SH. 1993. Cloning and characterization of a gene whose product is a trans-activator of anthrax toxin synthesis. J. Bacteriol. 175:5329–38

18. Candela T, Fouet A. 2006. Poly-gamma-glutamate in bacteria. Mol. Microbiol. 60:1091–98

19. Drysdale M, Heninger S, Hutt J, Chen Y, Lyons CR, Koehler TM. 2005. Capsule synthesis by Bacillus anthracis is required for dissemination in murine inhalation anthrax. EMBO J. 24:221–27

20. Perego M, Hoch JA. 2008. Commingling regulatory systems following acquisition of virulence plasmids by Bacillus anthracis. Trends Microbiol. 16:215–21

22. Pannucci J, Okinaka RT, Williams E, Sabin R, Ticknor LO, Kuske CR. 2002. DNA sequence conservation between the Bacillus anthracis pXO2 plasmid and genomic sequence from closely related bacteria. BMC Genomics 3:34

22. Van der Auwera GA, Andrup L, Mahillon J. 2005. Conjugative plasmid pAW63 brings new insights into the genesis of the Bacillus anthracis virulence plasmid pXO2 and of the Bacillus thuringiensis plasmid pBT9727. BMC Genomics 6:103

23. Sun J., Collier J.R. Disulfide Bonds in the Ectodomain of Anthrax Toxin Receptor 2 Are Required for the Receptor-Bound Protective-Antigen Pore to Function. 2010. PLoS.

24. Drum CL, Yan SZ, Bard J, Shen YQ, Lu D, et al. (2002) Structural basis for the activation of anthrax adenylyl cyclase exotoxin by calmodulin. Nature 415: 396–402.

25. Leppla SH (1982) Anthrax toxin edema factor: A bacterial adenylate cyclase that increases cyclic AMP concentrations of eukaryotic cells. Proc Natl Acad Sci U S A 79: 3162–3166.

26. Milne, J. C., D. Furlong, P. C. Hanna, J. S. Wall, and R. J. Collier. 1994. Anthrax protective antigen forms oligomers during intoxication of mammalian-cells. J. Biol. Chem. 269:20607–20612.

27. Abrami, L., S. H. Liu, P. Cosson, S. H. Leppla, and F. G. van der Goot. 2003. Anthrax toxin triggers endocytosis of its receptor via a lipid raft mediated clathrin-dependent process. J. Cell Biol. 160:321–328.

28. Gordon, V. M., S. H. Leppla, and E. L. Hewlett. 1988. Inhibitors of receptor-mediated endocytosis block the entry of Bacillus-anthracis adenylate-cyclase toxin but not that of bordetella-pertussis adenylatecyclase toxin. Infect. Immun. 56:1066–1069.

29. Benson, E. L., Huynh, P. D., Finkelstein, A.&Collier, R. J. (1998) *Biochemistry* 37, 3941–3948.

30. Friedlander, A. M. (1986) *J. Biol. Chem.* 261, 7123–7126.

31. Petosa, C., Collier, R. J., Klimpel, K. R., Leppla, S. H. & Liddington, R. C. (1997) Crystal structure of the anthrax toxin protective antigen *Nature* 385, 833–838.

32. Darling RG, Catlett CL, Huebner KD, Jarrett DG (2002) Threats in bioterrorism. I: CDC category A agents. Emerg Med Clin North Am 20: 273–309.

33. Puziss, M., L. C. Manning, J. W. Lynch, E. Barclay, I. Abelow, and G. G. Wright. 1963. Large-scale production of protective antigen of *Bacillus anthracis* in anaerobic cultures. Appl. Microbiol. 11:330–334.

34. Taft, S. C., and A. A. Weiss. 2008. Neutralizing activity of vaccine-induced antibodies to two *Bacillus anthracis* toxin components, lethal factor and edema factor. Clin. Vaccine Immunol. 15:71–75.

35. Geier, D. A., and M. R. Geier. 2002. Anthrax vaccination and joint related adverse reactions in light of biological warfare scenarios. Clin. Exp. Rheumatol. 20:217–220.

36. Geier, M. R., and D. A. Geier. 2004. Gastrointestinal adverse reactions following anthrax vaccination: an analysis of the Vaccine Adverse Events Reporting System (VAERS) database. Hepatogastroenterology 51:762–767.

37. Greidanus, T. G., and B. A. Honl. 2002. Delayed-type hypersensitivity reaction to anthrax vaccine. Mil. Med. 167:74–75.

38. Muniz, A. E. 2003. Lymphocytic vasculitis associated with the anthrax vaccine: case report and review of anthrax vaccination. J. Emerg. Med. 25:271– 276.

39. Pittman, P. R., P. H. Gibbs, T. L. Cannon, and A. M. Friedlander. 2001. Anthrax vaccine: short-term safety experience in humans. Vaccine 20:972– 978.

40. Swanson-Biearman, B., and E. P. Krenzelok. 2001. Delayed life-threatening reaction to anthrax vaccine. J. Toxicol. Clin. Toxicol. 39:81–84.

41. Vasudev, M., and M. C. Zacharisen. 2006. New-onset rheumatoid arthritis after anthrax vaccination. Ann. Allergy Asthma Immunol. 97:110–112.

42. Min, D.H., Tang, W.J., Mrksich, M. (2004). Chemical screening by mass spectrometry to identify inhibitors of anthrax lethal factor. Nature Biotech 22:717-723.

43. Rogers MS, Cryan LM, Habeshian KA, Bazinet L, Caldwell TP, et al. (2012) A FRET-Based High Throughput Screening Assay to Identify Inhibitors of Anthrax Protective Antigen Binding to Capillary Morphogenesis Gene 2 Protein. PLoS ONE 7(6): e39911. doi:10.1371/journal.pone.0039911.

44. Bradley, K. A., Mogridge, J., Mourez, M., Collier, R. J. & Young, J. A. (2001) Nature 414 **,** 225–229.

45. Scobie HM, Rainey GJ, Bradley KA, Young JA (2003) Human capillary morphogenesis protein 2 functions as an anthrax toxin receptor. Proc Natl Acad Sci U S A 100: 5170–5174.

46. Lee, J.-O., Rieu, P., Arnaout,M. A. & Liddington, R. C. Crystal structure of the A-domain from the a subunit of integrin CR3 (CD11b/CD18). Cell 80, 631–635 (1995).

47. Bonuccelli, G., F. Sotgia, P. G. Frank, T. M. Williams, C. J. de Almeida, H. B. Tanowitz, P. E. Scherer, K. A. Hotchkiss, B. I. Terman, B. Rollman, A. Alileche, J. Brojatsch, and M. P. Lisanti. 2005. ATR/TEM8 is highly expressed in epithelial cells lining Bacillus anthracis' three sites of entry: implications for the pathogenesis of anthrax infection. Am. J. Physiol. Cell Physiol. 288:C1402–C1410.

48. Rmali, K. A., M. A. Al-Rawi, C. Parr, M. C. Puntis, and W. G. Jiang. 2004. Upregulation of tumour endothelial marker-8 by interleukin-1beta and its impact in IL-1β induced angiogenesis. Int. J. Mol. Med. 14:75–80.

49. Wigelsworth, D. J.; Krantz, B. A.; Christensen, K. A.; Lacy, D. B.; Juris, S. J.; Collier, R. J. Binding Stoichiometry and Kinetics of the Interaction of a Human Anthrax Toxin Receptor, CMG2, with Protective Antigen. J. Biol. Chem. 2004. 279, 23349–23356.

50. Petosa, C., Collier, R. J., Klimpel, K. R., Leppla, S. H. & Liddington, R. C. Crystal structure of the anthrax toxin protective antigen. Nature 385, 833–838 (1997).

51. Lacy, D. B.,Wigelsworth, D. J., Scobie, H. M., Young, J. A. & Collier, R. J. Crystal structure of the von Willebrand factor A domain of human capillary morphogenesis protein 2: An anthrax toxin receptor. Proc. Natl Acad. Sci. USA 101, 6367–6372 (2004).

52. Liu, S., Crown, D., Miller-Randolph, S., Moayeri, M., Wang, H., Hu, H., Morley, T., and Leppla, S. H. (2009) Capillary morphogenesis protein-2 is the major receptor mediating lethality of anthrax toxin in vivo. Proc. Natl. Acad. Sci. U.S.A. 106, 12424–12429.

53. Deuquet, J., Lausch, E., Guex, N., Abrami, L., Salvi, S., Lakkaraju, A., Ramirez, M. C. M., Martignetti, J. A., Rokicki, D., Bonafe, L., Superti-Furga, A., and Van Der Goot, F. G. (2011) Hyaline fibromatosis syndrome inducing mutations in the ectodomain of anthrax toxin receptor 2 can be rescued by proteasome inhibitors. *EMBO Mol Med* **3**, 208–221

54. Cunningham, K., Lacy, D.B., Mogridge, J. & Collier, R.J. Mapping the lethal factor and edema factor binding sites on oligomeric anthrax protective antigen. Proc. Natl. Acad. Sci. USA 99, 7049–7053 (2002).

55. Miller, C. J., Elliott, J. L., and Collier, R. J. (1999) Anthrax protective antigen: prepore-to-pore conversion. *Biochemistry* **38**, 10432–10441

56. De Leon, J., Jiang, G., Ma, Y., Rubin, E., Fortune, S., and Sun, J. (2012)

Mycobacterium tuberculosis ESAT-6 Exhibits a Unique Membrane-interacting Activity That Is Not Found in Its Ortholog from Non-pathogenic Mycobacterium smegmatis. *J Biol Chem* **287**, 44184–44191

57. Jacquez, P., Lei, N., Weigt, D., Xiao, C., and Sun, J. (2013) Expression and purification of the functional ectodomain of human anthrax toxin receptor 2 in Escherichia coli Origami B cells with assistance of bacterial Trigger Factor. *Protein Expr Purif* **95C**, 149–155.

60. Sun, J., Vernier, G., Wigelsworth, D. J., and Collier, R. J. (2007) Insertion of anthrax protective antigen into liposomal membranes: effects of a receptor. *J Biol Chem* 282, 1059–1065.

61. Qa'dan M, Christensen KA, Zhang L, Roberts TM, Collier RJ (2005) Membrane insertion by anthrax protective antigen in cultured cells. Mol Cell Biol. 25:5492–5498.

62. Milne, J. C., Furlong, D., Hanna, P. C., Wall, J. S., and Collier, R. J. (1994) Anthrax protective antigen forms oligomers during intoxication of mammalian cells. *J Biol Chem* 269, 20607–20612.

63. Rainey, G. J. A., Wigelsworth, D. J., Ryan, P. L., Scobie, H. M., Collier, R. J., and Young, J. A. T. (2005) Receptor-specific requirements for anthrax toxin delivery into cells. *Proc Natl Acad Sci USA* 102, 13278–13283.

64. Lacy, D. B., D. J. Wigelsworth, R. A. Melnyk, S. C. Harrison, and R. J. Collier. 2004. Structure of heptameric protective antigen bound to an anthrax toxin receptor: a role for receptor in pH-dependent pore formation. Proc. Natl. Acad. Sci. USA 101:13147–13151.

65. Lakowicz, Joseph, R. Principles of Fluorescence Spectroscopy. New York: Springer Science+Business Media, LLC, 2006. Print.

Glossary

<OPTIONAL: If Glossary not used, delete the entire page, including the following page break>

Appendix

<OPTIONAL: If Appendix not used, delete the entire page including the following page break>

Vita

Pedro Raymundo Jacquez Valenzuela was born August 14, 1985 in El Paso, Texas, United States of America. He was raised in El Paso, but also in a small town outside of Chihuhua, San Guillermo, Chihuahua, Mexico, by his maternal grandparents. He is the youngest of five and only male. He obtained his Bachelors of Science in Microbiology from the University of Texas at El Paso on May, 2008.

In 2009, he joined the graduate program at the University of Texas at El Paso under the mentorship of Dr. Jianjun Sun. He and Dr. Sun worked on understanding the role and mechanism of the disulfide bonds in the Anthrax Toxin Receptor towards anthrax pathogenesis. He was also a teaching assistant for senior level undergraduate laboratories and also a lecturer for a non-since major's biology course. He also participated in many conferences including the Rio Grande American Society of Microbiology (2011, 2014), the Annual Biomedical Research Conference for Minority Students (2014), and the Health Minorities and Heal Disparities Grantees' Conference (2014), in which he presented posters and gave talks about his research.

Finally, as a graduate student, he published two first authors articles on his research, and contributed to another publication as a co-author. After graduating he plans on joining a research company or government laboratory, to study and develop better ways to detect bacterial pathogenesis.

Permanent address: 420 McCarthy Ave

El Paso, Texas 79915

This dissertation was typed by Pedro Raymundo Jacquez.